

MODERN DECOMPRESSION ALGORITHMS: MODELS, COMPARISONS, AND STATISTICS

B.R. Wienke
Los Alamos National Laboratory
Applied Physics Division
Los Alamos, N.M. 87545

INTRODUCTION

Overview

The subject of decompression theory in general is the study of pressure changes in blood and tissues. And today, we still do not know all the answers, maybe even less, the questions. But for diving applications, we need regimens and protocols to stage diver ascents on any given breathing mixture, and that is the focus of this short paper. Deterministic models are broadly categorized as dissolved gas (Haldane) or dual phase (dissolved plus free gas), and both are described and contrasted. Probabilistic models fold risk parameters over statistical data in maximum likelihood, employing metrics and variables computed directly in deterministic models. The statistics associated with decompression illness (DCI) are also discussed.

Pressure And Decompression Modeling

The physics, biology, engineering, physiology, medicine, and chemistry of diving center on pressure, and pressure changes. The average individual is subjected to atmospheric pressure swings of 3% at sea level, as much as 20% a mile in elevation, more at higher altitudes, and all usually over time spans of hours to days. Divers and their equipment can experience compressions and decompressions orders of magnitude greater, and within considerably shorter time scales. While the effects of pressure change are readily quantified in physics, chemistry, and engineering applications, the physiology, medicine, and biology of pressure changes in living systems are much more complicated.

Increases in pressure with increasing depth impose many of the limitations in diving, applying equally well to the design of equipment. Early divers relied on their breathholding ability, while later divers used diving bells. Surface supplied air and SCUBA are rather recent innovations. With increasing exposure times and depths, divers encountered physiological and medical problems constraining activity, with decompression illness (DCI) perhaps the most noteworthy. By the 1880s, bubbles were noted in animals subjected to pressure reduction. By the 1900s, bubbles were postulated as the cause of DCI in divers and caisson workers.

Within that postulate and driven by the need to optimize diver and aviator safety and time, decompression modeling has consolidated early rudimentary schedules into present more sophisticated tables and models. As basic knowledge and understanding of the biophysical effects of pressure change increase, so will the validity, reliability, and range of applicable models and algorithms used to stage diver ascents.

GAS DYNAMICS AND PHASE TRANSFER

Dissolved Phase Transfer

All gases dissolve in all liquids, but actual solubilities range over many orders of magnitude. Considering inert gases at room temperature, for illustration, the solubility of xenon in *n*-octane, a hydrocarbon liquid, is 470 times that of helium in water. Gas solubilities can vary much more for complex solutes and solvents. The solubility of the anesthetic gas halothane in olive oil is more than 10^6 times the solubility of common gases in liquid mercury. Inert gases such as helium and nitrogen are readily soluble in tissue and blood, and their solubility can fuel bubble growth with reduction in ambient pressure, a concern for decompressing divers.

Denoting the ambient partial pressure of a gas, p , and its solubility, S , in a liquid, the relative concentration of the dissolved gas component, c , is given by Henry's law,

$$c = Sp. \tag{1}$$

The corresponding *tension*, or dissolved gas partial pressure, is also p at equilibrium. By convention, partial pressures usually refer to the free gas phase, while tensions refer to the dissolved gas phase, though some folks use them interchangeably. When there exist differences, or *gradients*, between gas partial pressures and/or tensions across regions of

varying concentration or solubility, gases will diffuse until partial pressures are equal, in short, move from regions of higher partial pressures to regions of lower partial pressures, regardless of the phases (free or dissolved) of the components. This movement is the crux of the decompression problem in divers and aviators, and modeling this movement is central to the formulation of decompression tables and dive computer algorithms.

Gas is driven across the tissue-blood interface by the gradient, but the rate at which bulk tissue transfers gas also depends on the blood flow rate and the degree of vascularity. Then both blood perfusion rate and gas diffusion rate contribute to the overall transfer process.

Perfusion Controlled Transport

Exchange of dissolved tissue and blood gas, controlled by blood flow rates across regions of varying concentration or solubility, is driven by the local tissue-blood gradient, that is, the difference between the arterial blood tension, p_a , and the instantaneous tissue tension, p , assuming that blood flow rates are considerably slower than gas diffusion rates across the regions. Such behavior is modeled in time, t , by simple classes of exponential response functions, bounded by p_a and the initial value of p , denoted p_i . These multitissue functions satisfy a differential *perfusion* rate equation,

$$\frac{\partial p}{\partial t} = -\lambda (p - p_a) , \quad (2)$$

and take the form, tracking both dissolved gas buildup and elimination symmetrically,

$$p - p_a = (p_i - p_a) \exp(-\lambda t) , \quad (3)$$

$$\lambda = \frac{.6931}{\tau} , \quad (4)$$

with perfusion constant, λ , defined by the tissue half-time, τ . Compartments with 2, 5, 10, 20, 40, 80, 120, 180, 240, 360, 480, and 720 minute half-times, τ , are employed, and half-times are independent of pressure.

In a series of dives or multiple stages, p_i and p_a represent extremes for each stage, or more precisely, the initial tension and the arterial tension at the beginning of the next stage. Stages are treated sequentially, with finishing tensions at one step representing initial tensions for the next step, and so on. Exposures are controlled through critical tensions, M , such that, throughout the dive,

$$p \leq M . \quad (5)$$

Diffusion Controlled Transport

Exchange of dissolved tissue and blood gas, controlled by diffusion across regions of varying concentration or solubility, is also driven by the local tissue-blood gradient, but solutions to the diffusion equation control transport. In simple planar geometry, the diffusion equation can be cast,

$$D \frac{\partial^2 p}{\partial x^2} = \frac{\partial p}{\partial t} , \quad (6)$$

with D the diffusion coefficient. As in the perfusion case, solutions depend on initial values, and also on boundary conditions. Tissue is separated into intravascular and extravascular regions for application of boundary conditions, with the tissue tension, p , equal to the arterial tension, p_a , at the tissue-blood interface. Solving and applying initial and boundary conditions, and then averaging the solutions over the spatial region, of thickness, l , there obtains,

$$p - p_a = (p_i - p_a) \frac{8}{\pi^2} \sum_{n=1}^{\infty} \frac{1}{(2n-1)^2} \exp(-\alpha_{2n-1}^2 Dt) , \quad (7)$$

with,

$$\alpha_{2n-1} = \frac{(2n-1)\pi}{l} . \quad (8)$$

A decay constant, κ , fitted to exposure data, is related to the diffusion coefficient, D ,

$$\kappa = \frac{\pi^2 D}{l^2} = .007928 \text{ min}^{-1} , \quad (9)$$

in the exponential expansion, and plays a similar role to λ in the perfusion controlled case. The diffusion expansion looks like a weighted sum of multitissue perfusion functions with decay constants, $(2n - 1)^2 \kappa$. A diffusion equivalent half-time, ω , is simply defined,

$$\omega = \frac{.6931}{\kappa} = 87.4 \text{ min} , \quad (10)$$

so that halftimes, ω_{2n-1} , in the weighted expansion, are given by,

$$\omega_{2n-1} = \frac{\omega}{(2n - 1)^2} . \quad (11)$$

As before, p_i and p_a represent extremes for each stage. Critical gradients, G , control diving through the constraint,

$$p - p_a \leq G , \quad (12)$$

Free Phase Transfer

To satisfy thermodynamic laws, bubbles in blood and tissue assume spherical shapes in the absence of external or mechanical (distortion) pressures. Bubbles entrain free gases because of a thin film, exerting surface tension pressure on the gas, of magnitude, $2\gamma/r$, with γ the Laplacian surface tension and r the bubble radius. Hydrostatic pressure balance requires that the pressure inside the bubble, Π ,

$$\Pi = \sum_{j=1}^J \pi_j , \quad (13)$$

with π_j bubble partial pressures of component (free) gases, exceed ambient pressure, P , by the surface tension pressure, $2\gamma/r$,

$$\Pi = P + \frac{2\gamma}{r} , \quad (14)$$

At small radii, surface tension pressure is greatest, and at large radii, surface tension pressure is least.

Gases will also diffuse into or out of a bubble according to differences in gas partial pressures inside and outside the bubble, whether in free or dissolved phases outside the bubble. In the former case, the gradient is termed *free - free*, while in the latter case, the gradient is termed *free - dissolved*. Unless the surface tension, γ , is identically zero, there is always a gradient tending to force gas out of the bubble, thus making the bubble collapse on itself because of surface tension pressure. If surrounding external pressures on bubbles change in time, however, bubbles may grow or contract.

Bubbles grow or contract according to the strength of the free-free or free-dissolved gradient, and it is the latter case which concerns divers under decompression. The radial rate at which bubbles grow or contract is roughly given by,

$$\frac{\partial r}{\partial t} = \frac{DS}{r}(Q - \Pi) , \quad (15)$$

with D and S tissue diffusivity and solubility, and total tissue tension, Q , the sum of component dissolved gas tensions,

$$Q = \sum_{j=1}^J p_j , \quad (16)$$

as before. A critical radius, r_c , separating growing from contracting bubbles is given by,

$$r_c = \frac{2\gamma}{Q - P} \quad (17)$$

and bubbles with radius $r > r_c$ will grow, while bubbles with radius $r < r_c$ will contract. Limiting bubble growth and impact upon nerves and circulation are issues when decompressing divers and aviators. The interplay between tissue tension and bubble growth is further complicated with ascent, since ambient pressure changes in time (depending on ascent rate).

CRITICAL TENSIONS AND PHASE VOLUMES

Critical Tensions

To maximize the rate of uptake or elimination of dissolved gases, the *gradient*, simply the difference between p_i and p_a , is maximized by pulling the diver as close to the surface as possible. Exposures are limited by requiring that the perfusion-dominated tissue tensions, p , never exceed criticality, M , for instance, written for each tissue compartment in the US Navy approach employing 5, 10, 20, 40, 80, and 120 *minute* tissue halftimes, τ ,

$$M = M_0 + \Delta M d \quad , \quad (18)$$

with,

$$M_0 = 152.7\tau^{-1/4} \quad , \quad (19)$$

$$\Delta M = 3.25\tau^{-1/4} \quad , \quad (20)$$

as a function of depth, d , for ΔM the change per unit depth.

Surfacing values, M_0 , are principal concerns in nonstop diving, while values at depth, $\Delta M d$, concern decompression diving. In both cases, the staging regimen tries to pull the diver as close to the surface as possible, in as short a time as possible. By contrast, free phase (bubble) elimination gradients, as seen, *increase* with depth, directly opposite to dissolved gas elimination gradients which *decrease* with depth. In actuality, decompression is a playoff between dissolved gas buildup and free phase growth, tempered by body ability to eliminate both. But dissolved gas models cannot handle both, so there are problems when extrapolating outside tested ranges.

In absolute pressure units, the corresponding critical gradient, G , is given by,

$$G = \frac{M}{.79} - P = 1.27 M - P \quad , \quad (21)$$

with P ambient pressure, and M critical nitrogen pressure. In bubble theories, supersaturation is limited by the critical gradient, G . In decompressed gel experiments, Strauss suggested that $G \approx 20$ *fsw* at ambient pressures less than a few atmospheres. Other studies suggest, $14 \leq G \leq 30$ *fsw*, as a range of critical gradients (G -values).

In diffusion-dominated approaches, the tissue tension is often limited by a single, depth-dependent criterion, such as,

$$M = \frac{709 P}{P + 404} \quad , \quad (22)$$

a continuous parameterization lying between fixed gradient and multitissue schemes.

Controlling Tissues

Blood rich, well perfused, aqueous tissues are usually thought to be *fast* (small τ), while blood poorer, scarcely-perfused, lipid tissues are thought to be *slow* (large τ), though the spectrum of halftimes is not correlated with actual perfusion rates in critical tissues. As reflected in relationship above, critical parameters are obviously larger for faster tissues. The range of variation with compartment and depth is not insignificant. Fast compartments control short deep exposures, while slow compartments control long shallow, decompression, and saturation exposures.

As is well known, bounce exposures are often limited by a depth-time law of the form,

$$d t_n^{1/2} \leq C \quad , \quad (23)$$

with t_n the nonstop time limit, and $400 \leq C \leq 500$ *fsw min*^{1/2}. One can obtain the corresponding tissue constant, λ , controlling the exposure at depth d , for nonstop time t_n , by differentiating the tissue equation with respect to depth, d , and setting the result to zero. With $p_a = 0.79 (d + 33)$ at sea level, there results,

$$1 - \exp(-\lambda t_n) (1 + 2 \lambda t_n) = 0 \quad . \quad (24)$$

Corresponding critical tensions, M , are then easily obtained from the tissue equation using d , λ , and t_n . In the above case, the transcendental equation is satisfied when,

$$\lambda t_n = 1.25 \quad , \quad (25)$$

thus providing a means to estimate controlling tissue half-time at depth for corresponding nonstop time limits.

Time Remaining

Time remaining before a stop or surfacing, time at a stop, or surface interval before flying can all be obtained by inverting the tissue equation. Taking the perfusion equation, and denoting the limiting critical tension at some desired stage (lower ambient pressure), M , the initial tension, p_i , and the instantaneous tension at that particular time, p , at stage, p_a , the limiting time, t , follows from,

$$t = \frac{1}{\lambda} \ln \left[\frac{p_i - p_a}{p - p_a} \right] \tag{26}$$

as the inversion of the tissue equation in time.

The nonstop time limit, t_n , follows by replacing the instantaneous tension, p , with the (limiting) critical tension, M , that is,

$$t_n = \frac{1}{\lambda} \ln \left[\frac{p_i - p_a}{M - p_a} \right] \tag{27}$$

while time remaining, t_r , at level, p_a , before ascension to new level with limiting critical tension, M , is given by,

$$t_r = \frac{1}{\lambda} \ln \left[\frac{p - p_a}{M - p_a} \right] , \tag{28}$$

with p the instantaneous tension now the initial tension. These hold for each compartment, λ . Across all compartments, the smallest t_n limits time at the present level when ascent is permitted, while the largest t_r prescribes wait time at the present level when ascent is not permitted. Table 1 lists compartment time limits using the critical tensions, M_0 , for the six compartments, $\tau = 5, 10, 20, 40, 80,$ and 120 min , that is, $M_0 = 104, 88, 72, 58, 52, 51 \text{ fsw}$. Note the blank entries in the Table correspond to depths less than the critical tension, so tissue loading to that critical tension is not possible.

Table 1. Compartment Time Limits At Depth.

$\tau \text{ (min)}$	5	10	20	40	80	120
$M_0 \text{ (fsw)}$	104	88	72	58	52	51
$d \text{ (fsw)}$						
40					198	269
50				95	123	173
60			100	65	91	129
70			51	50	73	103
80		56	37	41	61	87
90		30	30	34	52	75
100	31	22	25	30	46	66
110	16	18	22	26	41	59
120	12	15	19	24	37	53
130	10	13	17	21	34	48
140	9	12	16	20	31	44
150	8	11	14	18	29	41
160	7	10	13	17	27	38
170	6	9	12	16	25	35
180	6	8	11	15	23	33
190	5	8	11	14	22	31
200	5	7	10	13	21	30

Generally, the t_n are monotonically decreasing functions of depth, while t_r are monotonically increasing functions of depth, for fixed M .

Saturation Curve And Separated Phase

In elegant experiments, using both animals and humans, subjects were first saturated at various pressures, Q , then decompressed to lower absolute pressures, P , and closely checked for bends development. Various values of Q and P can be determined in a controlled *titration*, that is, by holding one variable fixed and changing the other very slightly

over times spans of a day, or more. In analyzing this saturation data, it is possible to draw a linear relationship, in the hyperbaric regime, separating bends from no bends for ranges of P and Q . For instance, The line takes the form, in fsw ,

$$Q = \zeta P + \xi , \quad (29)$$

with an approximate spread over different studies, depending on statistics,

$$1.20 \leq \zeta \leq 1.40 \quad (30)$$

$$7.5 fsw \leq \xi \leq 15.3 fsw , \quad (31)$$

and a range of ambient pressures, P ,

$$33 fsw \leq P \leq 300 fsw . \quad (32)$$

In the hypobaric regime, $P < 33 fsw$, recent studies suggest that the air saturation curve passes through the origin as ambient pressure drops, behavior predicted within phase models and discussed further on. Wienke deduced a general form, in (fsw),

$$Q = \left[2.37 - \exp \left(-\frac{11.1}{P} \right) \right] P \quad (33)$$

using the permissible bubble (Doppler) excess as a phase limit point. For all exposures, $0 \leq P \leq \infty$, the supersaturation, Q , is bounded, with linear asymptotic behavior for large P , and zero intercept for small P . That is,

$$\lim_{P \rightarrow 0} Q \rightarrow 2.37 P \rightarrow 0 \quad (34)$$

$$\lim_{P \rightarrow \infty} Q \rightarrow \left[2.37 - 1 + \frac{1.11}{P} \right] P \rightarrow 1.37 P + 11.1 \quad (35)$$

Hennessy and Hempleman, and later Yount and Hoffman, established the linear titration curve for the data assuming that the same critical volume of released gas provokes mild attacks of decompression sickness. Such analyses offer explanations for changes in signs and symptoms which follow changes in the nature of the exposure to pressure. Findings press dissolved gas approaches. While the above titration expression is compatible with broad trends, it is clear that dissolved gas limiters, such as tensions, are often not the best critical flags. Indicators such as the volume fraction of separated gas are not only more natural, but seem to correlate more strongly with experiment. Computational algorithms, coupling phase equilibration or observed numbers of bubbles to critical volumes, offer more rational physical alternatives to the matrix of critical tensions. The critical volume hypothesis is an important development in decompression modeling, and certainly extends to breathing mixtures other than air.

Critical Phase Volumes

The rate at which gas inflates in tissue depends upon both the excess bubble number, Λ , and the supersaturation gradient, G . The critical volume hypothesis requires that the integral of the product of the two must always remain less than some limit point, αV , with α a proportionality constant. Accordingly this requires,

$$\int_0^\infty \Lambda G dt \leq \alpha V , \quad (36)$$

for bubble number excess, Λ , an approximately linear function of excitation seed radius (difference) on compression-decompression, ΔP ,

$$\Lambda = N(r_i - r) \quad (37)$$

with N , β seed constants, r_i , r seed sizes, and V the limiting gas volume. Assuming that tissue gas gradients are constant during decompression, t_d , while decaying exponentially to zero afterwards, and taking limiting condition of the equal sign, yields for a bounce dive,

$$\Lambda G(t_d + \lambda^{-1}) = \alpha V . \quad (38)$$

With compression-decompression, ΔP , the excitation radius, r , follows from lipid and aqueous equations-of-state (EOS),

$$\frac{1}{r} = \frac{1}{r_i} + \frac{\Delta P}{\zeta} \quad (39)$$

where r_i are excitation radii at initial pressure, P_i , for final pressure, P , so that, $\Delta P = P - P_i$, and with, $130 \mu m fsw \leq \zeta \leq 180 \mu m fsw$,

$$\zeta = 87 \left[1 + 1.21 \left(\frac{P}{T} \right)^{1/3} \right] \exp(-11.4z/T) \quad (40)$$

for z the elevation in multiples of 1,000 ft , and T the absolute temperature. At sea level, consistent fits to air exposure data suggest that, $r_i = .65 \text{ microns}$. From the above, $r \leq r_i$, as, $P \geq P_i$, that is, smaller seeds grow on decompression. With all exposures, the integral must be evaluated iteratively over component decompression stages, maximizing each G while satisfying the constraint equation. In the latter case, t_d is the sum of individual stage times plus interstage ascent times, assuming the same interstage ascent speed, v . Employing the above iteratively, and one more constant, δ , defined by,

$$\delta = \frac{\gamma_c \alpha V}{\gamma \beta r_i N} = 7500 \text{ fsw min} , \quad (41)$$

we have,

$$\left[1 - \frac{r}{r_i} \right] G(t_d + \lambda^{-1}) = \delta \frac{\gamma}{\gamma_c} = 522.3 \text{ fsw min} , \quad (42)$$

from the Spencer bounce and Tektite saturation data. A set of critical phase volume gradients, G , appears in Table 2 below, and the gradient representation, G , is of the usual form,

$$G = G_0 + \Delta G d \quad (43)$$

at depth, d .

Table 2. Critical Phase Volume Gradients.

halftime τ (min)	threshold depth δ (fsw)	surface gradient G_0 (fsw)	gradient change ΔG
2	190	151.0	.518
5	135	95.0	.515
10	95	67.0	.511
20	65	49.0	.506
40	40	36.0	.468
80	30	27.0	.417
120	28	24.0	.379
240	16	23.0	.329
480	12	22.0	.312

For repetitive diving, the gradients, G , above are replaced with a reduced set, \bar{G} , with the property,

$$\bar{G} \leq G . \quad (44)$$

tending to reduce bottom time for repetitive activities and exposures. Because of this constraint, the approach is termed a reduced gradient bubble model. The terms, ΛG and $\Lambda \bar{G}$, differ by effective bubble elimination during the previous surface interval. To maintain the phase volume constraint during multidiving, the elimination rate must be downscaled by a set of bubble growth, regeneration, and excitation factors, cumulatively designated, ξ , such that,

$$\bar{G} = \xi G . \quad (45)$$

A conservative set of bounce gradients, G , can be employed for multiday and repetitive diving, provided they are reduced by ξ . Three bubble factors, η , reduce the driving gradients to maintain the the phase constraint. In trying to retrofit the reduction parameters, η , to Haldane critical tensions and nonstop time limits, it is advantageous to use a slightly different picture for the multidiving fraction, ξ ,

$$\xi = \gamma_{rg}\eta^{rg} + \gamma_{rp}\eta^{rp} + \gamma_{rd}\eta^{rd} \quad (46)$$

for γ a set of weighting factors normalized,

$$\gamma_{rg} + \gamma_{rp} + \gamma_{rd} = 1 \quad (47)$$

and specific reduction factors, η^j , of a general Gaussian form ($j = rg, rp, ex$),

$$\eta^j = 1 - \alpha_j \exp \left[-\frac{(t_{sur} - \beta_j)^2}{4\beta_j^2} \right]$$

with α_j and β_j weighting fractions and Doppler relaxation halftimes following repetitive, reverse profile, and multiday diving, and α_j functions of depth differences on reverse dives and depth in general. Likelihood regression analysis is used to fit parameters to data, with typical ranges,

$$0.15 \leq \alpha_{rp} \leq .65$$

$$0.25 \leq \alpha_{rd} \leq .85$$

$$0.10 \leq \alpha_{rg} \leq 0.40$$

$$15 \text{ min} \leq \beta_{rp} \leq 130 \text{ min}$$

$$25 \text{ min} \leq \beta_{rd} \leq 190 \text{ min}$$

$$2 \text{ days} \leq \beta_{rg} \leq 24 \text{ days}$$

Ascent Staging

Clearly, from all of the foregoing, the dominant modes for staging diver ascents depend upon the preponderance of separated or dissolved phases in the tissues and blood, their coupling, and their relative time scales for elimination. This is (and will always be) the central consideration in staging hyperbaric or hypobaric excursions to lower ambient pressure environments. The dynamics of elimination are directly opposite. To eliminate dissolved gases (the central tenet of Haldane decompression theory), the diver is brought as close as possible to the surface. To eliminate free phases (the coupled tenet of bubble decompression theory), the diver is maintained at depth to both crush bubbles and squeeze gas out by diffusion across the bubble film surface. Since both phases must be eliminated, the problem is a playoff in staging. In mathematical terms, staging is a minimax problem, and one that requires full blown dual phase models, exposure data, and some consensus of what is an acceptable level of DCI incidence.

Many competing transfer pathways exist between tissues and blood (dissolved and free gas phases in both). The central problem of the table and meter designer is to stage ascents so that both free and dissolved phases are removed from tissues by the capillary system in optimal fashion. This is equally as difficult since we know little about the composition and susceptibility of tissue sites, blood perfusion rates, and geometries for modeling gas transfer. And even if we did, the complexity of the model and the computing power of our largest and fastest supercomputers would mitigate solutions. For instance, the complexity of ascent rates, tissue tensions, and ambient pressure on bubble growth, with pressures and tensions varying widely on ascent, is not a simply tracked quantity in diving exposures even when we know all the variables.

Attempts to track free phases within patently dissolved phase models may not optimize, but still can be mocked up for consistency with phase dynamics. One approach is to slow ascent rates and/or introduce safety stops strategically.

As far as net gas exchange is concerned, most combinations of stops and rates can be equivalenced to almost any other set at given pressure, so there is always some leeway. Growth minimization and free phase elimination favor slow ascents.

Based on suggestions at an American Academy Of Underwater Sciences ascent workshop, recorded by Lang and Egstrom, discretionary safety stops for 2-4 *min* in the 10-20 *fsw* zone are recommended. Calculations reported by Wienke and Lewis, and summarized in Tables 3 and 4, underscore the bases of the suggestions for a number of reasons. Relative changes in three computed trigger points, tissue tension, separated phase volume, and bubble radius, are listed for six compartments following a nominal bounce dive to 120 *fsw* for 12 *min*, with and without a safety stop at 15 *fsw* for 3 *min*. Stop procedures markedly restrict bubble and phase volume growth, while permitting insignificant levels of dissolved gas buildup in the slow tissues. The reduction in growth parameters far outstrips any dissolved gas buildup in slow compartments, and faster compartments naturally eliminate dissolved gases during the stop, important for deeper diving. Staging diver ascents is a minimax problem. To eliminate dissolved gas, the diver is brought as close to the surface as possible. To eliminate free phases, the diver is kept at depth. Obviously, staging diver ascents with dual phase (free and dissolved gases) treatments is a payoff. Both must be eliminated, but timescales and pressures for both are different.

Table 3. Relative Changes In Critical Parameters After Safety Stop

τ (<i>min</i>) halftimes	tissue tension relative change	critical volume relative change	bubble radius relative change
5	-21%	-34%	-68%
10	-11%	-24%	-39%
20	-6%	-11%	-24%
40	-2%	-8%	-18%
80	1%	3%	-2%
120	2%	4%	1%

Safety stop time can be added to bottom time for additional conservatism, but the effect of neglecting stop time is also small, as seen in Table 4. A stop at 15 *fsw* for 2 *min* is roughly equivalent to more than halving the standard ascent rate at depths in excess of 120 *fsw*. Procedures such as this, as well as reduced nonstop time limits, appear beneficial in multiday, multilevel, and repetitive diving. A safety stop near 15 *fsw* is easier than 10 *fsw* in adverse water conditions, such as surge and surface disturbances. Slower ascent rates afford additional advantages, but safety stops in the 2-4 *min* range are easier and more efficient.

Table 4. Comparative Surfacing Tissue Tensions

τ (<i>min</i>) Halftimes	Surfacing Tension (<i>fsw</i>) 120 <i>fsw</i> /15 <i>min</i>	Surfacing Tension (<i>fsw</i>) 120 <i>fsw</i> /12 <i>min</i> 15 <i>fsw</i> /3 <i>min</i>	Surfacing Tension (<i>fsw</i>) 120 <i>fsw</i> /15 <i>min</i> 15 <i>fsw</i> /3 <i>min</i>
5	101.5	77.0	79.7
10	87.5	73.0	78.1
20	66.9	59.0	64.0
40	49.9	45.7	49.2
80	39.0	36.9	38.9
120	34.9	33.5	34.8

At altitude the same procedures can be employed, with depths, ascent rates, and stops conservatively scaled by the altitude correction factors (ratio of sea level pressure to ambient pressure at altitude) when using tables for which critical tensions need extrapolation at reduced ambient pressure. Tables with critical tensions fitted to altitude data have their own rules, as do meters.

Generally, bubble growth and excitation are compounded at altitude because of reduced pressure. The modeling work of Wienke, Gernhardt and Lambertsen underscores this fact, indicating why critical tension models often fall short in hypobaric applications. Bubbles grow faster as they get bigger, and as pressure drops. With decreased pressure, bubbles will also expand by Boyle's law. Bigger bubbles are not as constricted by Laplacian film tension, while reduced

pressure supports a faster rate of tissue gas diffusion into the bubble itself. Lanphier and Lehner performed extensive aerial decompression studies with goats, concluding that aerial decompression sickness strongly resembles underwater decompression sickness following saturation exposure. For ranging profiles followed by decompression to reduced ambient pressure, a high incidence of chokes was noted. Chokes is thought to result from microemboli interfering with pulmonary function. It is easy to speculate that rapid decompression to reduced pressure contributes to the buildup and growth of pulmonary emboli for the same reasons. Lanphier also concluded that slow tissue ($\tau \geq 80 \text{ min}$) compartments do not correlate with chokes, suggesting that pulmonary microemboli are linked to fast compartments. Clearly, such an assertion also points out differences between types of decompression sickness, inferred critical tissue half-lives, and bubble formation time scales. Chokes and limb bends result from different critical insults, at different places, and over possibly different time scales.

The point to be made here in all cases is simple. Increased offgassing pressures reduce bubble growth rates dramatically in shallow zones, while impacting dissolved gas buildup in the slowest compartments minimally. Fast compartments also offload gas during safety stops, important for repetitive diving. Stops and slow ascent rates are always advisable, but particularly in multiexposures.

ALTITUDE SIMILARITY AND EXPOSURE ASYMPTOTICS

Critical Extrapolations

Lower ambient pressures at elevation, and the lesser density of fresh water in smaller degree, affect gas uptake and elimination rates in tissues and blood. If critical critical tensions are employed to limit exposures, an immediate question centers upon from their extrapolation and testing at altitude. Certainly, from their form a linear extrapolation of the critical tensions seems obvious, indeed just such an extrapolation of the US Navy critical tensions was proposed and tested by Bell and Borgwardt. Buhlmann, employing a different set of halftimes and critical tensions, also extended the Haldane algorithm to altitudes near 10,000 *ft*. Along with reduced critical tensions at altitude, reduced nonstop time limits, compared to sea level, are a natural consequence.

Another approach reduces critical tensions exponentially with decreasing ambient pressure. Such an extrapolation turns the curves down through the origin at zero ambient pressure. Intuitively, an exponential extrapolation of critical tensions through the origin is more conservative than the linear extrapolation, since corresponding critical tensions for given ambient pressure are smaller, also noted by others. If the extrapolation of critical tensions is allowed to follow the same exponential decrease of ambient pressure with altitude, then the ratio of the critical tension over ambient pressure, R , remains constant. Nonstop time limits in the exponential scheme are also smaller than corresponding time limits in the linear scheme. As seen in Table 5, atmospheric pressure falls off approximately 1 *fsw* for every 1,000 *ft* of elevation. Exponential extrapolations of critical tensions have been tested, and serve as the operational basis of altitude procedures suggested by many others. Correlations of altitude chokes data for goats with constant ratio, R , trigger points have also been established, along with similar suggestions for the nitrogen washout data in aviators.

Altitude Procedures And Equivalent Sea Level Depth (ESLD)

Tables and meters designed for sea level need be conservatively modified at altitude if possible, otherwise, not employed. Decomputer and table use are best left to manufacturer and designer discretions, but in any case, modification of critical tensions is central to any Haldane altitude algorithm. We will describe a general technique and, for discussion purposes, the US Navy dive tables (or derivative) will suffice.

Present diving schedules are based to large extent on the model discussed in the previous section, constraining activities so that M or R are never compromised. An approach to altitude diving that is roughly as conservative as the tested schemes of original researchers, holds the ratios, R , constant at altitude, forcing altitude exposures to be *similar* to sea level exposures. Such similarity will force M to decrease exponentially with increasing altitude, keeping R constant with commensurate exponential reduction in the ambient pressure, P . Constant R extrapolations of this sort should be confined to nominal diving activities, certainly not heavy repetitive, decompression, nor saturation exposures.

The sought ratio constancy, R , at altitude induces a necessary scaling of actual depth to *equivalent sea level depth* (ESLD) for table entry, while all times remain unchanged. Actual depths at altitude are multiplied by factors, α , called altitude correction factors, which are just the ratios of sea level atmospheric pressure to altitude atmospheric pressure, multiplied by the specific density of fresh water (0.975). Neglect of the specific density scaling is a conservative convenience, and one of minimal impact on these factors. Today, wrist altimeters facilitate rapid, precise estimation of α on site. They can be estimated from the *barometer* equation (shortly discussed) and are always greater than one. Table

5 lists correction factors at various altitudes, z , ranging to 10,000 ft . Up to about 7,000 ft elevation, $\alpha \approx 1 + 0.038 h$, with h measured in multiples of 1,000 ft , that is, $z = 1000 h$. The higher one ascends to dive, the deeper is his relative exposure in terms of sea level equivalent depth. Correction factors increase rapidly above 10,000 ft . As seen in Table 5, P and α are reciprocally related, inverses actually. Again, time is measured directly, that is, correction factors are only applied to underwater depths, ascent rates, and stops.

Table 5. Altitude Correction Factors And US Navy Altitude Groups.

altitude, or change z (ft)	atmospheric pressure P_h (fsw)	correction factor α	penalty group on arrival at altitude	permissible group for ascension to altitude
0	33.00	1.00		
1,000	31.9	1.04	A	L
2,000	30.8	1.07	B	K
3,000	29.7	1.11	B	J
4,000	28.5	1.16	C	I
5,000	27.5	1.20	D	H
6,000	26.5	1.24	E	G
7,000	25.4	1.29	E	F
8,000	24.5	1.34	F	E
9,000	23.6	1.39	G	D
10,000	22.7	1.45	H	C

The similarity rule for altitude table modification and applying correction factors to calculations is straightforward. Convert depths at altitude to sea level equivalent depths through multiplication by α . Convert all table sea level stops and ascent rates back to actual altitude through division by α . Ascent rates are always less than 60 fsw/min , while stops are always less than at sea level. Thus, a diver at 60 fsw at an elevation of 5,000 ft uses a depth correction of 72 fsw , taking $\alpha = 1.2$. Corresponding ascent rate is 50 fsw/min , and a stop at 10 fsw at sea level translates to 8 fsw . A capillary gauge at altitude performs these depth calculations automatically, and on the fly, as described below. Here the 3% density difference between salt and fresh water is neglected. Neglecting the 3% density correction is conservative, because the correction decreases equivalent depth by 3%. The effect on ascent rate or stop level is not on the conservative side, but is so small that it can be neglected in calculations anyway. Correction factors, β , are used to scale depths at altitude to sea level equivalence for use in standard tables. The factors are always greater than one, and are simply the ratios of sea level atmospheric pressures to atmospheric pressures at elevation, multiplied by the specific density, η , of fresh water,

$$\beta = \eta \left[\frac{33}{P_h} \right] = .975 \exp(0.0381h) = .975\alpha \tag{48}$$

with h measured in multiples of 1,000 ft elevation.

If a diver has equilibrated with ambient pressure at any elevation, than any reduction in ambient pressure will put the diver in a repetitive group, merely because tissue tensions exceed ambient pressure. If the original and new pressures are specified, it is possible to estimate tissue saturation and, hence, repetitive group for the excursion. Similar comments apply to pressure reductions following any diving activity, with sea level diving the usual bill of fare. These considerations are treated as follows.

At sea level, each repetitive group represents an increment of tissue pressure over ambient ($P_0 = 33 fsw$). For the US Navy tables, this increment is 2 fsw (absolute). If we compute the difference between sea level pressure pressure and altitude pressure, and then scale the difference by the ratio of sea level atmospheric pressure to that altitude atmospheric pressure (correction factor α), we can estimate the repetitive group in which a sea level diver finds himself following immediate ascent to altitude. These group specifications are listed in column 4 of Table 5, and represent penalty time for the excursion to altitude, Entries were computed using sea level as the baseline, but are also appropriate (conservative) for any excursion between differing elevations.

In similar fashion, excursions to higher altitude following diving are limited by tissue critical tensions, and minimal repetitive group designators can be attached to any planned excursion. For the 120 minute compartment, the surfacing critical tension (sea level) is 51 fsw . On the safer side, we take 44 fsw as the limiting tension, convert it to an absolute

tension of 60 fsw (44/.79), and then inversely scale it to altitude by the ratio of sea level pressure to altitude pressure, that is, α . The resulting limiting tensions at altitude can then be converted to standard US Navy groups which are tabulated in column 5 of Table 5. Entries represent maximum permissible groups for immediate altitude excursions, and do not account for any travel time. Thus a diver would have to wait some length of time after a dive, until he dropped into the permissible group category, before ascending. The *D – Group* rule for flying after diving is seen as a subcase for an altitude excursion to 9,000 ft (maximum cabin pressure). The question of altitude delay is an interesting one, a subject of recent discussions.

Extended Haldane Staging

Operational consistency of Haldane table and meter algorithms is also of interest here, and part of the reason is reflected in Table 6, which contrasts surfacing critical tensions, M_0 , for a number of meter algorithms. Entries were estimated (computed) from quoted meter nonstop time limits, t_n , using the 5, 10, 20, 40, 80, and 120 min compartments for convenience of illustration, that is to say that arbitrary τ and M_0 can be fitted to any set of nonstop time limits. Ascent and descent rates of 60 fsw/min were also employed in calculations. The Workman, Buhlmann, and Spencer critical surfacing tensions are fixed, while the equivalent Wienke-Yount surfacing critical tensions vary, depending on repetitive exposure. Entries are also representative of critical tensions employed in related tables.

Table 6. Table And Meter Surfacing Critical Tensions (M_0).

halftime τ (min)	Workman M_0 (fsw)	Spencer M_0 (fsw)	Buhlmann M_0 (fsw)	Wienke-Yount M_0 (fsw)
5	104	100	102	100-70
10	88	84	82	81-60
20	72	68	65	67-57
40	58	53	56	57-49
80	52	51	50	51-46
120	51	49	48	48-45

A glance at Table 6 underscores the operational consistency of classes of Haldane meter algorithms, with the Wienke-Yount approach effectively reducing critical tensions in multiding applications as the simplest meter implementation of a dual phase model. The variation in M_0 within the same compartments is relatively small. Table 7 collates the corresponding nonstop time limits, t_n , for completeness.

Table 7. Table And Meter Nonstop Time Limits (t_n).

depth d (fsw)	Workman t_n (min)	Spencer t_n (min)	Buhlmann t_n (min)	Wienke-Yount t_n (min)
30		225	290	250
40	200	135	125	130
50	100	75	75	73
60	60	50	54	52
70	50	40	38	39
80	40	30	26	27
90	30	25	22	22
100	25	20	20	18
110	20	15	17	15
120	15	10	15	12
130	10	5	11	9

Variation in the nonstop limits is greater than in the critical tensions, with the US Navy set the most liberal. Using the equivalent depth approach within the similarity method, the nonstop limits in Table 7 can be extrapolated to altitude with correction factors. Correction factors are routinely employed to scale (multiply) actual depths for direct table entry (ESLD). Scaled depths at altitude are always greater than actual depths, as discussed in altitude procedures, so time limits are less. If correction factors are applied to the Wienke-Yount critical tensions in Table 6, virtually the same set of nonstop limits at altitude result. Reduction in nonstop time limits is some 2% – 3% for each 1,000 ft of elevation. This is no real surprise, since phase volume models recover Haldane predictions for short (nonstop) exposures.

MIXED GASES AND DECOMPRESSION

Mixtures

Mixed breathing gases, across a spectrum of underwater activities, have been utilized successfully, mostly mixtures of nitrogen, helium, and oxygen, differing from pure air, and lately those with higher oxygen content than air (*enriched*), which can be used in shallow diving. Non-enriched mixtures of nitrogen/oxygen (nitrox), helium/oxygen (heliox), and helium/nitrogen/oxygen (trimix), of course, are employed commercially in deep and saturation diving. Recently, mixtures of hydrogen/oxygen (hydrox) have been tested. A closer look at these inert gases in a range of diving applications is illuminating, particularly gas properties, advantages and disadvantages, and interplay.

Biological Reactivities

Low pressure oxygen toxicity can occur if a gas mixture with 60% oxygen is breathed at 1 atm for 12 hours or more. Pulmonary damage, irritation, and coughing are manifestations (pulmonary toxicity). High pressure oxygen toxicity can occur when breathing pure oxygen at pressures greater than 1 atm for periods of minutes to hours, the lower the oxygen pressure the longer the time for symptoms to develop, and vice versa, as seen in Table 8 below. Twitching, convulsions, and dizziness are the symptoms (nervous system toxicity). On the other hand, if oxygen pressures fall below .16 atm, unconsciousness may result. Low levels of oxygen inhibit tissue cell metabolic function (hypoxia). Confusion and difficulty in maintaining coordination are milder symptoms. Severe hypoxia requires medical attention.

Table 8. Oxygen Depth-Time Limits (t_x).

oxygen depth d (fsw)	air depth d (fsw)	time limit t_x (min)
10	50	240
15	75	150
20	100	110
25	125	75
30	150	45
35	175	25
40	200	10

Clearly a constraint in mixed gas diving is the oxygen partial pressure. Inspired partial pressures of oxygen must remain below 1.6 atm (52.8 fsw) to prevent central nervous system (CNS) toxicity, and above .16 atm (5.3 fsw) to prevent hypoxia. This window, so to speak, is confining, some 1.44 atm (47.5 fsw). Denoting the mole fraction of oxygen, f_{O_2} , the upper and lower limits of this window, d_{max} and d_{min} , can be written (fsw),

$$\eta d_{max} = \frac{52.8}{f_{O_2}} - P_h \quad , \quad (49)$$

$$\eta d_{min} = \frac{5.3}{f_{O_2}} - P_h \quad , \quad (50)$$

$$\eta d_{max} - \eta d_{min} = \frac{47.5}{f_{O_2}} \quad , \quad (51)$$

with η the specific density (with respect to sea water) and with working depths, d , limited by d_{max} and d_{min} ,

$$d_{min} \leq d \leq d_{max} \quad . \quad (52)$$

For fresh water, $\eta = .975$, and for sea water, $\eta = 1.000$. Certainly up to about 7,000 ft elevation, the lower limit, d_{min} , is no real constraint, with the surface accessible as the limit.

Another factor inhibiting performance underwater is inert gas narcosis, particularly at increasing ambient pressure. Although the common gases nitrogen and helium associated with diving are physiologically inert under normal atmospheric conditions, they both exhibit anesthetic properties as their partial pressures increase. The mechanism is

not completely understood, but impaired carbon dioxide diffusion in the lungs, increased oxygen tension, fear, and related chemical reactions have all been implicated in the past. With 80/20 mixtures, symptom onset for nitrogen is near 100 *fsw*, and very much deeper for helium, in the 1,000 *fsw* range. Symptoms range from light headedness to unconsciousness at the extreme.

Nitrogen is limited as an inert gas for diving. Increased pressures of nitrogen beyond 200 *fsw* lead to excessive euphoria, and reduced mental and physical functional ability, while beyond 600 *fsw* loss of consciousness results. Individual tolerances vary widely, often depending on activity. Symptoms can be marked at the beginning of a deep dive, gradually decreasing with time. Flow resistance and the onset of turbulence in the airways of the body increase with higher breathing gas pressure, considerably reducing ventilation with nitrogen-rich breathing mixtures during deep diving. Oxygen is also limited at depth for the usual toxicity reasons. Dives beyond 300 *fsw* requiring bottom times of hours need employ lighter, more weakly reacting, and less narcotic gases than nitrogen, and all coupled to reduced oxygen partial pressures.

Comparative Properties

A number of inert gas replacements have been tested, such as hydrogen, neon, argon, and helium, with only helium and hydrogen performing satisfactorily on all counts. Because it is the lightest, hydrogen has elimination speed advantages over helium, but, because of the high explosive risk in mixing hydrogen, helium has emerged as the best all-around inert gas for deep and saturation diving. Helium can be breathed for months without tissue damage. Argon is highly soluble and heavier than nitrogen, and thus a very poor choice. Neon is not much lighter than nitrogen, but is only slightly more soluble than helium. Of the five, helium is the least and argon the most narcotic inert gas under pressure.

Saturation and desaturation speeds of inert gases are inversely proportional to the square root of their atomic masses. Hydrogen will saturate and desaturate approximately 3.7 times faster than nitrogen, and helium will saturate and desaturate some 2.7 times faster than nitrogen. Differences between neon, argon, and nitrogen are not significant for diving. Comparative properties for hydrogen, helium, neon, nitrogen, argon, and oxygen are listed in Table 9. Solubilities, *S*, are quoted in *atm*⁻¹, weights, *A*, in *atomic mass units (amu)*, and relative narcotic potencies, *v*, are dimensionless (referenced to nitrogen in observed effect). The least potent gases have the highest index, *v*.

Table 9. Inert Gas And Oxygen Molecular Weights, Solubilities, and Narcotic Potency.

	<i>H</i> ₂	<i>He</i>	<i>Ne</i>	<i>N</i> ₂	<i>Ar</i>	<i>O</i> ₂
<i>A (amu)</i>	2.02	4.00	20.18	28.02	39.44	32.00
<i>S (atm</i> ⁻¹ <i>)</i>						
blood	.0149	.0087	.0093	.0122	.0260	.0241
oil	.0502	.0150	.0199	.0670	.1480	.1220
<i>v</i>	1.83	4.26	3.58	1.00	0.43	

The size of bubbles formed with various inert gases depends upon the amount of gas dissolved, and hence the solubilities. Higher gas solubilities promote bigger bubbles. Thus, helium is preferable to hydrogen as a light gas, while nitrogen is preferable to argon as a heavy gas. Neon solubility roughly equals nitrogen solubility. Narcotic potency correlates with lipid (fatty tissue) solubility, with the least narcotic gases the least soluble. Different uptake and elimination speeds suggest optimal means for reducing decompression time using helium and nitrogen mixtures. Following deep dives beyond 300 *fsw* breathing helium, switching to nitrogen is without risk, while helium elimination is accelerated because the helium tissue-blood gradient is increased when breathing an air mixture. By gradually increasing the oxygen content after substituting nitrogen for helium, the nitrogen uptake can also be kept low. Workable combinations of gas switching depend upon the exposure and the tissue compartment controlling the ascent.

Mixed gas diving dates back to the mid 1940s, but proof of principle diving experiments were carried out in the late 50s. In 1945, Zetterstrom dove to 500 *fsw* using hydrox and nitrox as a travel mix, but died of hypoxia and DCI when a tender hoisted him to the surface too soon. In 1959, Keller and Buhlmann devised a heliox schedule to 730 *fsw* with only 45 *min* of decompression. Then, in 1962, Keller and Small bounced to 1,000 *fsw*, but lost consciousness on the way up due to platform support errors. Small and another support diver, Whittaker, died as a result. In 1965, Workman published decompression tables for nitrox and heliox, with the nitrox version evolving into

USN Tables. At Duke University Medical Center, the 3 man team of Atlantis III made a record chamber dive to 2250 *fsw* on heliox, and Bennett found that 10% nitrogen added to the heliox eliminated high pressure nervous syndrome (HPNS). In deep saturation diving, *normoxic* breathing mixtures of gases are often advantageously employed to address oxygen concerns. A normoxic breathing mixture, helium or nitrogen, reduces the oxygen percentage so that the partial pressure of oxygen at the working depth is the same as at sea level, the obvious concerns, again, hypoxia and toxicity. Critical tensions can be employed in helium saturation diving in much the same fashion as nitrogen diving. A critical tension, recall, is the maximum permissible value of inert gas tension (*M*-value) for a hypothetical tissue compartment with specified halftime. An approach to helium exchange in tissue compartments employs the usual nitrogen set with halftimes reduced by 2.7, that is, the helium halftimes are extracted from the nitrogen halftimes following division by 2.7, and the same critical tension is assumed for both gas compartments. Researchers have tested schedules based on just such an approach. Tissue tensions scale as the relative proportion of inert gas in any mixture. More so than in air diving, computational methods for mixed gas diving and decompression are often proprietary information in the commercial sector.

Helium (normal 80/20 mixture) nonstop time limits are shorter than nitrogen, but follow a $t^{1/2}$ law similar to nitrogen, that is, depth times the square root of the nonstop time limit is approximately constant. Using standard techniques of extracting critical tensions from the nonstop time limits, fast compartment critical tensions can be assigned for applications. Modern bubble models, such as the varying permeability model, have also been used strategically in helium diving.

Today, the three helium and nitrogen mixtures (nitrox, heliox, trimix) are employed for deep and saturation diving, with a tendency towards usage of enriched oxygen mixtures in shallow (recreational) diving. The use of enriched oxygen mixtures by recreational divers is the subject of controversy, aptly a concern over diver safety. Breathing mixture purity, accurate assessment of component gas ratios, oxygen toxicity, and appropriate decompression procedures are valid concerns for the mixed gas diver. Care, in the use of breathing mixtures, is to be underscored. Too little, or too much, oxygen can be disastrous. The fourth hydrogen mixture (hydrox) is much less commonplace.

Nitrox

Mixtures of oxygen and nitrogen with less oxygen than 21% (pure air) offer protection from oxygen toxicity in moderately deep and saturation diving. Moderately deep here means no more than a few hundred feet. Hypoxia is a concern with mixtures containing as much as 15% oxygen in this range. Saturation diving on oxygen-scarce nitrox mixtures is a carefully planned exposure. The narcotic effects of nitrogen in the 100 *fsw* to 200 *fsw* depth range mitigate against nitrox for deep diving.

Diving on enriched nitrox mixtures need be carefully planned exposures, but for opposite reason, that is, oxygen toxicity. Mixtures of 30% more of oxygen significantly reduce partial pressures of nitrogen to the point of down loading tissue tensions compared to air diving. If standard air decompression procedures are employed, enriched nitrox affords a diving safety margin. However, because of elevated oxygen partial pressures, a maximum permissible depth (floor) needs be assigned to any enriched oxygen mixture. Taking 1.6 *atm* (52.8 *fsw*) as the oxygen partial pressure limit, the floor for any mixture is easily computed. Enriched nitrox with 32% oxygen is floored at a depth of 130 *fsw* for diving, also called the oxygen limit point. Higher enrichments raise that floor proportionately.

Decompression requirements on enriched nitrox are less stringent than air, simply because the nitrogen content is reduced below 79%. Many equivalent means to schedule enriched nitrox diving exist, based on the standard Haldane critical tension approach. Air critical tensions can be employed with exponential buildup and elimination equations tracking the (reduced) nitrogen tissue gas exchange, or equivalent air depths (always less than the actual depths on enriched nitrox) can be used with air tables. The latter procedure ultimately relates inspired nitrogen pressure on a nitrox mixture to that of air at shallower depth (equivalent air depth). For instance, a 74/26 nitrox mixture at a depth of 140 *fsw* has an equivalent air depth of 130 *fsw* for table entry. Closed breathing circuit divers have employed the equivalent air depth approach for many years.

Heliox

The narcotic effects of nitrogen in the several hundred feet range prompted researchers to find a less reactive breathing gas for deeper diving. Tests, correlating narcotic effects and lipid solubility, affirm helium as the least narcotic of breathing gases, some 4 times less narcotic than nitrogen according to Bennett, and as summarized in Table 9. Deep saturation and extended habitat diving, conducted at depths of 1,000 *ft* or more on helium/oxygen mixtures by the US Navy, ultimately ushered in the era of heliox diving. For very deep and saturation diving above 700 *fsw* or so, heliox remains a popular, though expensive, breathing mixture.

Helium uptake and elimination can also be tracked with the standard Haldane exponential expressions employed for nitrogen, but with a notable exception. Corresponding helium halftimes are some 2.7 times faster than nitrogen for the same hypothetical tissue compartment. Thus, at saturation, a 180 *minute* helium compartment behaves like a 480 *minute* nitrogen compartment. All the computational machinery in place for nitrogen diving can be ported over to helium nicely, with the 2.7 scaling of halftimes expedient in fitting most helium data.

When diving on heliox, particularly for deep and long exposures, it is advantageous to switch to nitrox on ascent to optimize decompression time, as discussed earlier. The higher the helium saturation in the slow tissue compartments, the later the change to a nitrogen breathing environment. Progressive increases of nitrogen partial pressure enhance helium washout, but also minimize nitrogen absorption in those same compartments. Similarly, progressive increases in oxygen partial pressures aid washout of all inert gases, while also addressing concerns of hypoxia.

An amusing problem in helium breathing environments is the high-pitched voice change, often requiring electronic voice encoding to facilitate diver communication. Helium is also very penetrating, often damaging vacuum tubes, gauges, and electronic components not usually affected by nitrogen. Though helium remains a choice for deep diving, some nitrogen facilitates decompression, ameliorates the voice problem, and helps to keep the diver warm. Pure helium, however, can be an asphyxiant.

Trimix

Diving much below 1400 *fsw* on heliox is not only impractical, but also marginally hazardous. High pressure nervous syndrome (HPNS) is a major problem on descent in very deep diving, and is quite complex. The addition of nitrogen to helium breathing mixtures (trimix), is beneficial in ameliorating HPNS. Trimix is a useful breathing mixture at depths ranging from 500 *fsw* to 2,000 *fsw*, with nitrogen percentages usually below 10% in operational diving, because of narcotic effect.

Decompression concerns on trimix can be addressed with traditional techniques. Uptake and elimination of both helium and nitrogen can be limited by critical tensions. Using a basic set of nitrogen halftimes and critical tensions, and a corresponding set of helium halftimes approximately 3 times faster for the same nitrogen compartment, total inert gas uptake and elimination can be assumed to be the sum of fractional nitrogen and helium in the trimix breathing medium, using the usual exponential expressions for each inert gas component. Such approaches to trimix decompression were tested by researchers years ago, and many others after them.

Hydrox

Since hydrogen is the lightest of gases, it is reasonably expected to offer the lowest breathing resistance in a smooth flow system, promoting rapid transfer of oxygen and carbon dioxide within the lungs at depth. Considering solubility and diffusivity, nitrogen uptake and elimination rates in blood and tissue should be more rapid than nitrogen, and even helium. In actuality, the performance of hydrogen falls between nitrogen and helium as an inert breathing gas for diving.

Despite any potential advantages of hydrogen/oxygen breathing mixtures, users have been discouraged from experimenting with hydrox because of the explosive and flammable nature of most mixtures. Work in the early 1950s by the Bureau of Mines, however, established that oxygen percentages below the 3%-4% level provide a safety margin against explosive and flammability risks. A 97/3 mixture of hydrogen and oxygen could be utilized at depths as shallow as 200 *fsw*, where oxygen partial pressure equals sea level partial pressure. Experiments with mice also indicate that the narcotic potency of hydrogen is less than nitrogen, but greater than helium. Unlike helium, hydrogen is also relatively plentiful, and inexpensive.

Haldane Decompression Procedures

In the case of mixtures of gases (nitrogen, helium, hydrogen), the Haldane decompression procedures can be generalized in a straightforward manner, using a set of nitrogen critical tensions, M , and halftimes, τ , as the bases. Denoting gas species, $j = N_2, He, H_2$, atomic masses, A_j , and partial pressures, p_j , each component satisfies a Haldane tissue equation, with rate modified coefficient, λ_j , given by,

$$p_j - p_{aj} = (p_{ij} - p_{aj}) \exp(-\lambda_j t) , \quad (53)$$

for p_{aj} and p_{ij} ambient and initial partial pressures of the j^{th} species, and with decay constant, λ_j , related by Graham's law to the nitrogen coefficient, $\lambda_{N_2} = \lambda$, by,

$$\lambda_j = \left[\frac{A_{N_2}}{A_j} \right]^{1/2} \lambda . \quad (54)$$

Thus, for instance, one has,

$$\lambda_{He} = 2.7 \lambda , \quad (55)$$

$$\lambda_{H_2} = 3.7 \lambda . \quad (56)$$

In a mixture, the total tension, Π , is the sum of all J partial tensions, p_j ,

$$\Pi = \sum_{j=1}^J [p_{aj} + (p_{ij} - p_{aj}) \exp(-\lambda_j t)] \quad (57)$$

and the decompression requirement is simply,

$$\Pi = \sum_{j=1}^J p_j \leq M , \quad (58)$$

for all exposures. Denoting ambient partial pressures, p_{aj} , as a fraction, f_j , of total pressure, P , that is,

$$p_{aj} = f_j P , \quad (59)$$

it follows that,

$$f_{O_2} + \sum_{j=1}^J f_j = 1 \quad (60)$$

neglecting any carbon dioxide or water vapor in the mixture, of course. For 75/25 (enriched) nitrox, $f_{N_2} = .75$, for 90/10 heliox, $f_{He} = .90$, for 75/10/15 trimix, $f_{He} = .75$, $f_{N_2} = .10$, while for 95/5 hydrox, $f_{H_2} = .95$. For pure air obviously $f_{N_2} = 0.79$, as the common case. Clearly the treatment of breathing mixtures assumes a single critical tension, M , for each compartment, τ , in this case, extracted from the nitrogen data.

With enriched nitrox ($f_{N_2} < .79$), it is clear that the nitrogen decompression requirements are reduced when using the same set of M , that is, the air set of M are assumed to apply equally to both air and other nitrogen mixtures. The procedure has been applied to heliox, trimix, and hydrox mixtures in similar vein. One important constraint in any mixture is the oxygen content. Partial pressures of oxygen must be kept below 52.8 fsw (1.6 atm) to prevent toxicity, and above 5.3 fsw (.16 atm) to prevent hypoxia. Balancing diver mobility within this window at increasing depth is a delicate procedure at times.

Equivalent Air Depth (EAD)

In extending air tables to other breathing mixtures, an extrapolation based on critical tensions is the crux of the *equivalent air depth* (EAD) method. The equivalent air depth method for table use derives from the imposed equality of mixture and inert gas partial pressures, and is very similar to the altitude equivalent depth method, but is not the same. For instance, with nitrox mixtures, the usual case, the equivalent air depth, δ , is related to the effective depth, d , by requiring equality of nitrogen partial pressures for air and nitrogen mixture with mole fraction f_{N_2} ,

$$\delta = \frac{f_{N_2}}{.79} (P_h + d) - P_h. \quad (61)$$

At altitude, the effective depth, d , is the equivalent sea level depth described earlier. At sea level, the actual depth and effective depth are the same.

With enriched mixtures ($f_{N_2} < .79$), it is clear that the equivalent air depth, δ , is less than the effective depth, d , so that nitrogen decompression requirements are reduced when using δ to enter any set of air tables. Obviously, the same set of M are assumed to apply equally to both air and other mixture in the approach. At sea level, the above reduces,

$$\delta = \frac{f_{N_2}}{.79} (33 + d) - 33, \quad (62)$$

with d the actual depth, and has been utilized extensively in ocean diving.

Equivalent Mixture Depth (EMD)

The same procedure can be applied to arbitrary heliox, trimix, and hydrox mixtures in theory, basically an extrapolation from a reference (standard) table with the same gas components (helium, nitrogen, or hydrogen with oxygen). Denoting gas molar fractions in the standard (table) mixture, f_{sk} , with $k = N_2, He, H_2, O_2$, and molar fractions in the arbitrary mixture, f_k , we have for the K component mixture,

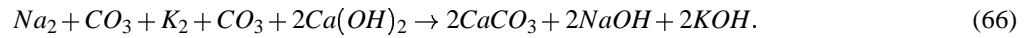
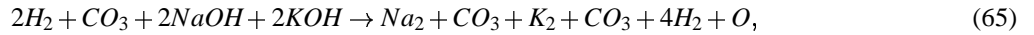
$$\delta = \frac{(1 - f_{O_2})}{(1 - f_{sO_2})}(P_h + d) - P_h. \quad (63)$$

This is the *equivalent mixture depth* (EMD). At altitude, the ESLD is first determined, followed by conversion to an EAD or EMD (conservative order).

Oxygen Rebreathing

As early as 1880, Fleuss developed and tested the first closed circuit, oxygen rebreathing system. At that time, of course, oxygen toxicity was not completely understood, though the effects of breathing pure oxygen were coupled to excitability and fever. In ensuing years, the apparatus was refined considerably, and was used by underwater combatants in World War II. During the 1950s, recreational divers used oxygen rebreathers. However, by the late 1950s, recreational divers switched to the popular open circuit device developed by Cousteau and Gagnan, thereby trading oxygen toxicity and caustic carbon dioxide concerns for decompression sickness and nitrogen narcosis. Today, rebreathers are witnessing a rebirth among technical divers. And, US Navy Underwater Demolition (UDT) and Sea, Air, Land (SEAL) Teams have continuously employed rebreathers for tactical operations.

In closed circuit systems, exhaled gas is kept in the apparatus, scrubbed of carbon dioxide by chemical absorbents, and then returned to the diver. No gas is released into the water (no bubbles). Gas consumption is related only to the physiological consumption of oxygen. Only a small amount of oxygen is required for extended exposures. Oxygen is taken directly from a breathing bag, and exhaled gas passes separately through an alkaline, absorbent material, where it is scrubbed of carbon dioxide. A typical reduction process involves water vapor, sodium and potassium hydroxide, and carbon dioxide in the reaction chain,



Rebreathers today last about 3 *hr*, using approximately 6 m^3 of oxygen and 4 *lbs* of absorbent. Because of oxygen toxicity, depth is a limitation for oxygen rebreathing. Depth limitation for pure oxygen rebreathing is near 20 *fsw*. Today, closed circuit mixed gas rebreathers blend inert gases with oxygen (lowering oxygen partial pressure) to extend depth limitations. Two cylinders, one oxygen and the other inert gas (or a premixed cylinder), are employed, and the mixture is scrubbed of carbon dioxide before return to the breathing bag.

Closed circuit oxygen scuba takes advantage of gas conservation, but is limited in dive depth and duration by oxygen toxicity effects. Open circuit scuba offers greater depth flexibility, but is limited in depth and duration by the inefficiency of gas utilization. To bridge this gap, semi-closed circuit mixed gas rebreathers were developed. The semi-closed circuit rebreather operates much like the closed circuit rebreather, but requires a continuous, or frequent, purge to prevent toxic inert gas buildup. Two cylinders of oxygen and inert gas (or one premixed), are charged with safe levels of both, usually corresponding to safe oxygen partial pressure at the maximum operating depth. Gas flow from the high pressure cylinders the breathing circuit is controlled by a regulator and nozzle, admitting a continuous and constant mass flow of gas determined by oxygen consumption requirements. The diver inhales the mixture from the breathing bag and exhales it into the exhalation bag. Pressure in the exhalation bag forces the gas mixture through the carbon dioxide scrubber, and from the scrubber back into the breathing bag for diver consumption. When gas pressure in the breathing circuit reaches a preset limit, a relief valve opens in the exhalation bag, purging excess gas into the water.

Oxygen rebreathing at high partial pressures can lead to central nervous system (or pulmonary) oxygen poisoning. It is thought that high pressure oxygen increases the production of oxygen free radicals disrupting cell function. The US Navy conducted research into safe depths and durations for oxygen diving, and concluded that there is very little risk of central nervous system oxygen toxicity when partial pressures of oxygen are maintained below 1.6 *atm*. Additionally, risk only increases slightly when oxygen partial pressures are maintained below 1.8 *atm*.

TABLES, METERS, AND BIOPHYSICAL MODELS

Protocols

Operational diving requires arbitrary numbers of dives to various depths over periods of hours, and often days. Once a standard set of decompression tables has been constructed, with bounce diving the simple case of nonstop decompression, a repetitive dive procedure is a necessity. After any air dive, variable amounts of dissolved and free residual nitrogen remain in body tissues for periods of 24 *hr*, and more. Similarly, elevated tissue tensions can promote, or sustain, bubble growth over the same time scales. This residual gas buildup (dissolved and free) will shorten the exposure time for subsequent repetitive dives. The longer and deeper the first dive, the greater the amount of residual tissue nitrogen affecting decompression on subsequent dives. Nonstop depth-time allowances for repetitive dives are reduced in such circumstance. Within bubble models, residual free gas phases are also included in procedures, imposing additional constraints on repetitive diving. The many possibilities are easily tracked in continuous time mode by computers, as mentioned, but tables face a more difficult task.

Tables

Considering only dissolved gases, one standard table approach, developed by Workman, groups combinations of depth and exposure times according to the surfacing tension in the slowest compartment. Then it is possible to account for desaturation during any arbitrary surface interval. The remaining excess nitrogen at the start of the next dive can always be converted into equivalent time spent at the deepest point of the dive. So called penalty time is then added to actual dive time to updated appropriate tissue tensions. Surfacing tensions in excess of 33 *fsw* (absolute) in the slowest compartment are assigned letter designations (groups), A to O, for each 2 *fsw* over 33 *fsw*. Any, and all, exposures can be treated in this manner. To credit outgassing, a Surface Interval Table, accounting for 2 *fsw* incremental drops in tensions in the slowest compartment, is also constructed. Such procedures are bases for the US Navy Air Decompression and Repetitive Surface Interval Tables, with the 120 *min* compartment (the slowest) controlling repetitive activity. Standard US Navy Tables provide safe procedures for dives up to 190 *fsw* for 60 *min*. Dives between 200 and 300 *fsw* were tested and reported in the exceptional exposure US Navy tables, including a 240 *min* compartment. The Swiss tables, compiled by Buhlmann, incorporate the same basic procedures, but with a notable exception. While the US Navy tables were constructed for sea level usage, requiring some safe extrapolation procedure to altitude, the Swiss tables are formulated and tested over a range of reduced ambient pressure. The controlling repetitive tissue in the Buhlmann compilation is the 635 *min* compartment. Similar approaches focusing on deep and saturation diving have resulted in decompression tables for helium-oxygen (heliox), helium-oxygen-nitrogen (trimix), and recent mixtures with some hydrogen (hydrox). Clearly, the USN and Swiss Repetitive Tables can be easily converted to other (longer or shorter) controlling tissues by arithmetic scaling of the 120 *min* or 635 *min* compartment to the desired controlling tissue half-time (simple ratio). To scale the USN Tables to 720 *min*, for instance, the repetitive intervals need only be multiplied by $720/120 = 6$.

While it is true that the table procedures just described are quite easily encoded in digital meters, and indeed such devices exist, digital meters are capable of much more than table recitations. Pulsing depth and pressure at short intervals, digital meters can monitor diving almost continuously, providing rapid estimates of any model parameter. When employing the exact same algorithms as tables, meters provide additional means to control and safety beyond table lookup. When model equations can be inverted in time, meters can easily compute time remaining before decompression, time at a stop, surface interval before flying, and optimal ascent procedure. Profiles can be stored for later analysis, and the resulting data bank used to tune and improve models and procedures. Considering utility and functionality, meter usage should increase in diving, supported by technological advance in computing power, algorithmic sophistication, and general acceptance, though it will probably be some time though before tables are supplanted.

Meters

On the heels of growing interest in underwater science and exploration following World War II, monitoring devices have been constructed to control diver exposure and decompression procedures. Devices, with records of varying success, include mechanical and electrical analogs, and within the past 15 years, microprocessor based digital computers. With inexpensive microprocessor technology, recent years have witnessed explosive growth in compact digital meters usage. All use the simple dissolved tissue gas model proposed by Haldane some 80 years ago, but given the sophistication of these devices, many feel that broader models can be incorporated into meter function today, increasing their range and flexibility. Although the biophysics of bubble formation, free and dissolved phase buildup and elimination is formidable, and not fully understood yet, contemporary models treating both dissolved and free phases, correlated with

existing data, and consistent with diving protocols might extend the utility of diving computers. An approach treating bubble nucleation, excitation, and growth in tissue and blood is needed. In the industry, such new models are termed bubble mechanical, because they focus on bubbles and their interactions with dissolved gas in tissue and blood.

Decompression computers are fairly inexpensive items these days. Basically a decompression meter is a microprocessor computer consisting of a power source, pressure transducer, analog to digital signal converter, internal clock, microprocessor chip with RAM (random access memory) and ROM (read only memory), and pixel display screen. Pressure readings from the transducer are converted to digital format by the converter, and sent to memory with the elapsed clock time for model calculations, usually every 1 - 3 *sec*. Results are displayed on the screen, including time remaining, time at a stop, tissue gas buildup, time to flying, and other model flag points, usually Haldanean (perfusion) tissue control variables. Some 3 - 9 volts is sufficient power to drive the computer for a couple of years, assuming about 100 dives per year. The ROM contains the model program (step application of model equations), all constants, and queries the transducer and clock. The RAM maintains storage registers for all dive calculations ultimately sent to the display screen. Dive computers can be worn on the wrist, incorporated in consoles, or even integrated into *heads-up* displays in masks.

Statistics point to an enviable track record of decompression meter usage in nominal diving activities, as well as an expanding user community. When coupled to slow ascent rates and safety stops, computer usage has witnessed a very low incidence rate of decompression sickness, below 0.01% according to some reports. Computers for nitrox are presently online today, with heliox and trimix units a rather simple modification of any nitrox unit, using existing decompression algorithms.

Decompression Models And Algorithms

Tables and schedules for diving at sea level can be traced to a model proposed in 1908 by the eminent English physiologist, John Scott Haldane. He observed that goats, saturated to depths of 165 feet of sea water (*f_{sw}*), did not develop decompression sickness (DCS) if subsequent decompression was limited limited to half the ambient pressure. Extrapolating to humans, researchers reckoned that tissues tolerate elevated dissolved gas pressures (tensions), greater than ambient by factors of two, before the onset of symptoms. Haldane then constructed schedules which limited the critical supersaturation ratio to two in hypothetical tissue compartments. Tissue compartments were characterized by their half-time, τ . Half-time is also termed *half-life* when linked to exponential processes, such as radioactive decay. Five compartments (5, 10, 20, 40, 75 *min*) were employed in decompression calculations and staged procedures for fifty years.

Some years following, in performing deep diving and expanding existing table ranges in the 1930s, US Navy investigators assigned separate limiting tensions (*M*-values) to each tissue compartment. Later in the 1950s and early 1960s, other USN investigators and divers, in addressing repetitive exposures and staging regimens for the first time, advocated the use of six tissues (5, 10, 20, 40, 80, 120 *min*) in constructing decompression schedules, with each tissue compartment again possessing its own limiting tension. Temporal uptake and elimination of inert gas was based on mechanics addressing only the macroscopic aspects of gas exchange between blood and tissue. Exact bubble production mechanisms, interplay of free and dissolved gas phases, and related transport phenomena were not quantified, since they were neither known nor understood. Today, we know more about dissolved and free phase dynamics, bubbles, and transport mechanisms, but still rely heavily on the Haldane model. Inertia and simplicity tend to sustain its popularity and use, and it has been a workhorse.

1. Bulk Diffusion Model

Diffusion limited gas exchange is modeled in time by a sum of exponential response functions, bounded by arterial and initial tissue tensions. However, instead of many tissue compartments, a single bulk tissue is assumed for calculations, characterized by a gas diffusion constant, *D*. Tissue is separated into intravascular (blood) and extravascular (cells) regions. Blood containing dissolved inert and metabolic gases passes through the intravascular zone, providing initial and boundary conditions for subsequent gas diffusion into the extravascular zone. Diffusion is driven by the difference between arterial and tissue tensions, according to the strength of a single diffusion coefficient, *D*, appropriate to the media. Diffusion solutions, averaged over the tissue domain, resemble a weighted sum over effective tissue compartments with time constants, $\lambda_{2n-1} = \alpha_{2n-1}^2 D$, determined by diffusivity and boundary conditions, with $\alpha_{2n-1} = (2n - 1)\pi/l$ for tissue thickness, *l*.

Applications fit the time constant, $K = \pi^2 D/l^2$, to exposure data, with a typical value employed by the Royal Navy given by, $K = 0.007928 \text{ min}^{-1}$, approximating the US Navy 120 *min* compartment used to control saturation,

decompression, and repetitive diving. Corresponding critical tensions in the bulk model,

$$M = \frac{709P}{P + 404}, \quad (67)$$

fall somewhere between fixed gradient and multitissue values. At the surface, $M = 53 \text{ fsw}$, while at 200 fsw , $M = 259 \text{ fsw}$. A critical gradient,

$$G = \frac{P(493 - P)}{(P + 404)}, \quad (68)$$

also derives from the above. Originally, a critical gradient, G , near 30 fsw was used to limit exposures. Such value is too conservative for deep and bounce exposures, and not conservative enough for shallow exposures. Hempleman introduced the above relationship, providing the means to parameterize bounce and saturation diving. Bulk diffusion models (BDM) are attractive because they permit the whole dive profile to be modeled with one equation, and because they predict a $t^{1/2}$ behavior of gas uptake and elimination. Nonstop time limits, t_n , are related to depth, d , by the bulk diffusion relationship,

$$dt_n^{1/2} = C, \quad (69)$$

with approximate range, $400 \leq C \leq 500 \text{ fsw min}^{1/2}$, linking nonstop time and depth simply through the value of C . For the US Navy nonstop limits, $C \approx 500 \text{ fsw min}^{1/2}$, while for the Spencer reduced limits, $C \approx 465 \text{ fsw min}^{1/2}$. In the Wienke-Yount model, $C \approx 400 \text{ fsw min}^{1/2}$.

2. Multitissue Model

Multitissue models (MTM), variations of the original Haldane model, assume that dissolved gas exchange, controlled by blood flow across regions of varying concentration, is driven by the local gradient, that is, the difference between the arterial blood tension and the instantaneous tissue tension. Tissue response is modeled by exponential functions, bounded by arterial and initial tensions, and perfusion constants, λ , linked to the tissue halftimes, τ , for instance, 1, 2, 5, 10, 20, 40, 80, 120, 180, 240, 360, 480, and 720 min compartments assumed to be independent of pressure.

In a series of dives or multiple stages, initial and arterial tensions represent extremes for each stage, or more precisely, the initial tension and the arterial tension at the beginning of the next stage. Stages are treated sequentially, with finishing tensions at one step representing initial tensions for the next step, and so on. To maximize the rate of uptake or elimination of dissolved gases the gradient, simply the difference between arterial and tissue tensions is maximized by pulling the diver as close to the surface as possible. Exposures are limited by requiring that the tissue tensions never exceed

$$M = M_0 + \Delta M d, \quad (70)$$

as a function of depth, d , for ΔM the change per unit depth. A set of M_0 and ΔM are listed in Table 10.

Table 10. Classical US Navy Surfacing Ratios And Critical Tensions.

halftime $\tau \text{ (min)}$	critical ratio R_0	critical tension $M_0 \text{ (fsw)}$	tension change ΔM
5	3.15	104	2.27
10	2.67	88	2.01
20	2.18	72	1.67
40	1.76	58	1.34
80	1.58	52	1.26
120	1.55	51	1.19

At altitude, some critical tensions have been correlated with actual testing, in which case, an effective depth, d , is referenced to the absolute pressure, P , (in fsw),

$$d = P - 33 \quad (71)$$

with surface pressure, P_h , at elevation, h , given by,

$$P_h = 33 \exp(-0.0381h) \quad (72)$$

for h in multiples of 1,000 ft . However, in those cases where critical tensions have not been tested, nor extended, to altitude, an exponentially decreasing extrapolation scheme, called similarity, has been employed. Extrapolations of critical tensions, below $P = 33 fsw$, then fall off more rapidly than in the linear case. A similarity extrapolation holds the ratio, $R = M/P$, constant at altitude. Estimating minimum surface tension pressure of bubbles near 10 fsw , as a limit point, the similarity extrapolation might be limited to 10,000 ft in elevation, and neither for decompression nor heavy repetitive diving.

Models of dissolved gas transport and coupled bubble formation are not complete, and all need correlation with experiment and wet testing. Extensions of basic (perfusion and diffusion) models can redress some of the difficulties and deficiencies, both in theory and application. Concerns about microbubbles in the blood impacting gas elimination, geometry of the tissue region with respect to gas exchange, penetration depths for gas diffusion, nerve deformation trigger points for pain, gas uptake and elimination asymmetry, effective gas exchange with flowing blood, and perfusion versus diffusion limited gas exchange, to name a few, motivate a number of extensions of dissolved gas models.

The multitissue model addresses dissolved gas transport with saturation gradients driving the elimination. In the presence of free phases, free-dissolved and free-blood elimination gradients can compete with dissolved-blood gradients. One suggestion is that the gradient be split into two weighted parts, the free-blood and dissolved-blood gradients, with the weighting fraction proportional to the amount of separated gas per unit tissue volume. Use of a split gradient is consistent with multiphase flow partitioning, and implies that only a portion of tissue gas has separated, with the remainder dissolved. Such a split representation can replace any of the gradient terms in tissue response functions.

If gas nuclei are entrained in the circulatory system, blood perfusion rates are effectively lowered, an impairment with impact on all gas exchange processes. This suggests a possible lengthening of tissue halftimes for elimination over those for uptake, for instance, a 10 *min* compartment for uptake becomes a 12 *min* compartment on elimination. Such lengthening procedure and the split elimination gradient obviously render gas uptake and elimination processes asymmetric. Instead of both exponential uptake and elimination, exponential uptake and linear elimination response functions can be used. Such modifications can again be employed in any perfusion model easily, and tuned to the data.

3. Thermodynamic Model

The thermodynamic model (TM) suggested by Hills, and extended by others, is more comprehensive than earlier models, addressing a number of issues simultaneously, such as tissue gas exchange, phase separation, and phase volume trigger points. This model is based on phase equilibration of dissolved and separated gas phases, with temporal uptake and elimination of inert gas controlled by perfusion and diffusion. From a boundary (vascular) thin zone, gases diffuse into the cellular region. Radial, one dimensional, cylindrical geometry is assumed as a starting point, though the extension to higher dimensionality is straightforward. As with all dissolved gas transfer, diffusion is controlled by the difference between the instantaneous tissue tension and the venous tension, and perfusion is controlled by the difference between the arterial and venous tension. A mass balance for gas flow at the vascular cellular interface, enforces the perfusion limit when appropriate, linking the diffusion and perfusion equations directly. Blood and tissue tensions are joined in a complex feedback loop. The trigger point in the thermodynamic model is the separated phase volume, related to a set of mechanical pain thresholds for fluid injected into connective tissue.

The full thermodynamic model is complex, though Hills has performed massive computations correlating with the data, underscoring basic model validity. Free phase dynamics (phase volume limits) impart deeper decompression staging formats, compared to considerations of critical tensions, and are characteristic of phase models. Full blown bubble models require the same, simply to minimize bubble excitation and growth.

4. Varying Permeability Model

The varying permeability model (VPM) treats both dissolved and free phase transfer mechanisms, postulating the existence of gas seeds (micronuclei) with permeable skins of surface active molecules, small enough to remain in solution and strong enough to resist collapse. The model is based upon laboratory studies of bubble growth and nucleation.

Inert gas exchange is driven by the local gradient, the difference between the arterial blood tension and the instantaneous tissue tension. Compartments with 1, 2, 5, 10, 20, 40, 80, 120, 240, 480, and 720 halftimes, τ , are again employed. While, classical (Haldane) models limit exposures by requiring that the tissue tensions never exceed the critical tensions, fitted to the US Navy nonstop limits, for example, the varying permeability model, however, limits the supersaturation gradient, through the phase volume constraint. An exponential distribution of bubble seeds, falling off with increasing bubble size is assumed to be excited into growth by compression-decompression. A critical radius, r_c , separates growing from contracting micronuclei for given ambient pressure, P_c . At sea level, $P_c = 33 \text{ fsw}$, $r_c = .8 \text{ microns}$. Deeper decompressions excite smaller, more stable, nuclei. Within this phase volume constraint, a set of nonstop limits, t_n , at depth, d , satisfy a modified law, $dt_n^{1/2} = 400 \text{ fsw min}^{1/2}$, with gradient, G , extracted for each compartment, τ , using the nonstop limits and excitation radius, at generalized depth, $d = P - 33 \text{ fsw}$. Table 11 summarize t_n , G_0 , ΔG , and δ , the depth at which the compartment begins to control exposures.

Table 11. Critical Phase Volume Time Limits.

depth $d \text{ (fsw)}$	nonstop limit $t_n \text{ (min)}$	depth $d \text{ (fsw)}$	nonstop limit $t_n \text{ (min)}$
30	250.	130	9.0
40	130.	140	8.0
50	73.	150	7.0
60	52.	160	6.5
70	39.	170	5.8
80	27.	180	5.3
90	22.	190	4.6
100	18.	200	4.1
110	15.	210	3.7
120	12.	220	3.1

Gas filled crevices can also facilitate nucleation by cavitation. The mechanism is responsible for bubble formation occurring on solid surfaces and container walls. In gel experiments, though, solid particles and ragged surfaces were seldom seen, suggesting other nucleation mechanisms. The existence of stable gas nuclei is paradoxical. Gas bubbles larger than $1 \mu\text{m}$ should float to the surface of a standing liquid or gel, while smaller ones should dissolve in a few *sec*. In a liquid supersaturated with gas, only bubbles at the critical radius, r_c , would be in equilibrium (and very unstable equilibrium at best). Bubbles larger than the critical radius should grow larger, and bubbles smaller than the critical radius should collapse. Yet, the Yount gel experiments confirm the existence of *stable* gas phases, so no matter what the mechanism, effective surface tension must be zero. Although the actual size distribution of gas nuclei in humans is unknown, these experiments in gels have been correlated with a decaying exponential (radial) distribution function. For a stabilized distribution accommodated by the body at fixed pressure, P_c , the excess number of nuclei excited by compression-decompression must be removed from the body. The rate at which gas inflates in tissue depends upon both the excess bubble number, and the supersaturation gradient, G . The critical volume hypothesis requires that the integral of the product of the two must always remain less than some volume limit point, αV , with α a proportionality constant.

5. Reduced Gradient Bubble Model

The RGBM departs from the VPM in a number of ways, abandoning gel parameterizations. The full blown RGBM also treats coupled perfusion-diffusion transport as a two step flow process, with blood flow (perfusion)

servicing as a boundary condition for tissue gas penetration by diffusion. Depending on time scales and rate coefficients, one or another (or both) processes dominate the exchange. However, for most meter implementations, perfusion is assumed to dominate, simplifying matters and permitting online calculations. Additionally, tissues and blood are naturally undersaturated with respect to ambient pressure at equilibration through the mechanism of biological inherent unsaturation (oxygen window), and the model includes this debt in calculations.

The RGBM assumes that a size distribution of seeds (potential bubbles) is present, and that a certain number is excited into growth by compression-decompression. An iterative process for ascent staging is employed to control the inflation rate of these growing bubbles so that their collective volume never exceeds a phase volume limit point. Gas mixtures of helium, nitrogen, and oxygen contain bubble distributions of different sizes, but possess the same phase volume limit point.

The RGBM postulates seeds with varying surfactant skins. Bubble skins are assigned lipid or aqueous equations-of-state (EOS). The size of seeds excited into growth is inversely proportional to the supersaturation gradient. The model assumes bubble skins are stabilized by surfactants over hour time scales, and that the seeds develop in the body. Bubble skins are probably molecularly activated, complex, biosubstances found throughout the body. Whatever the formation process, the model assumes the size distribution is exponentially decreasing in size, that is, more smaller seeds than larger seeds in exponential proportions.

The model incorporates a spectrum of tissue compartments, ranging from 1 *min* to 720 *min*, depending on gas mixture (helium, nitrogen, oxygen). Phase separation and bubble growth in slower compartments is a central focus in calculations, and the model uses nonstop time limits tuned to recent Doppler measurements, conservatively reducing them along the lines originally suggested by Spencer (and others), but within the phase volume constraint.

The RGBM reduces the phase volume limit in multiding by considering free phase elimination and buildup during surface intervals, depending on altitude, time, and depth of previous profiles. Repetitive, multiday, and reverse profile exposures are tracked and impacted by critical phase volume reductions over appropriate time scales. The model generates replacement bubble seed distributions on time scales of days, adding new bubbles to existing bubbles in calculations. Phase volume limit points are also reduced by the added effects of new bubbles.

The reduced gradient bubble model extends the varying permeability model to repetitive diving, by conservatively reducing the gradients, G . A conservative set of bounce gradients, G , can always be used for multiday and repetitive diving, provided they are multiplicatively reduced by a set of bubble factors, all less than one. Three bubble factors reduce the driving gradients to maintain the phases volume constraint. The first bubble factor reduces G to account for creation of new stabilized micronuclei over time scales of days. The second factor accounts for additional micronuclei excitation on reverse profile dives. The third bubble factor accounts for bubble growth over repetitive exposures on time scales of hours.

The RGBM and VPM are both diveware implementations, accessible on the Internet at various sites. Additionally, the RGBM has been encoded into a number of commercial decompression meter products.

6. Tissue Bubble Diffusion Model

The tissue bubble diffusion model (TBDM), according to Gernhardt and Vann, considers the diffusive growth of an extravascular bubble under arbitrary hyperbaric and hypobaric loadings. The approach incorporates inert gas diffusion across the tissue-bubble interface, tissue elasticity, gas solubility and diffusivity, bubble surface tension, and perfusion limited transport to the tissues. Tracking bubble growth over a range of exposures, the model can be extended to oxygen breathing and inert gas switching. As a starting point, the TBDM assumes that, through some process, stable gas nuclei form in the tissues during decompression, and subsequently tracks bubble growth with dynamical equations. Diffusion limited exchange is invoked at the tissue-bubble interface, and perfusion limited exchange is assumed between tissue and blood, very similar to the thermodynamic model, but with free phase mechanics. Across the extravascular region, gas exchange is driven by the pressure difference between dissolved gas in tissue and free gas in the bubble, treating the free gas as ideal. Initial nuclei in the TBDM have assumed radii near 3 *microns* at sea level, to be compared with .8 *microns* in the VPM and RGBM.

As in any free phase model, bubble volume changes become more significant at lower ambient pressure, suggesting a mechanism for enhancement of hypobaric bends, where constricting surface tension pressures are smaller

than those encountered in hyperbaric cases. Probabilistically, the model has been bootstrapped to statistical likelihood, correlating bubble size with decompression risk, a topic discussed further on. Then, a theoretical bubble dose of 5 ml correlates with a 20% risk of decompression sickness, while a 35 ml dose correlates with a 90% risk, with the bubble dose representing an unnormalized measure of the separated phase volume. Coupling bubble volume to risk represents yet another extension of the phase volume hypothesis, a viable trigger point mechanism for bends incidence.

Empirical Practices

Utilitarian procedures, entirely consistent with phase mechanics and bubble dissolution time scales, have been developed under duress, and with trauma, by Australian pearl divers and Hawaiian diving fishermen, for both deep and repetitive diving with possible in-water recompression for hits. While the science behind such procedures was not initially clear, the operational effectiveness was always noteworthy and could not be discounted easily. Later, the rationale, essentially recounted in the foregoing, became clearer.

Pearling fleets, operating in the deep tidal waters off northern Australia, employed Okinawan divers who regularly journeyed to depths of 300 fsw for as long as one hour, two times a day, six days per week, and ten months out of the year. Driven by economics, and not science, these divers developed optimized decompression schedules empirically. As reported by Le Messurier and Hills, deeper decompression stops, but shorter decompression times than required by Haldane theory, were characteristics of their profiles. Such protocols are entirely consistent with minimizing bubble growth and the excitation of nuclei through the application of increased pressure, as are shallow safety stops and slow ascent rates. With higher incidence of surface decompression sickness, as might be expected, the Australians devised a simple, but very effective, in-water recompression procedure. The stricken diver is taken back down to 30 fsw on oxygen for roughly 30 minutes in mild cases, or 60 minutes in severe cases. Increased pressures help to constrict bubbles, while breathing pure oxygen maximizes inert gas washout (elimination). Recompression time scales are consistent with bubble dissolution experiments.

Similar schedules and procedures have evolved in Hawaii, among diving fishermen, according to Farm and Hayashi. Harvesting the oceans for food and profit, Hawaiian divers make between 8 and 12 dives a day to depths beyond 350 fsw. Profit incentives induce divers to take risks relative to bottom time in conventional tables. Three repetitive dives are usually necessary to net a school of fish. Consistent with bubble and nucleation theory, these divers make their deep dive first, followed by shallower excursions. A typical series might start with a dive to 220 fsw, followed by 2 dives to 120 fsw, and culminate in 3 or 4 more excursions to less than 60 fsw. Often, little or no surface intervals are clocked between dives. Such types of profiles literally clobber conventional tables, but, with proper reckoning of bubble and phase mechanics, acquire some credibility. With ascending profiles and suitable application of pressure, gas seed excitation and any bubble growth are constrained within the body's capacity to eliminate free and dissolved gas phases. In a broad sense, the final shallow dives have been tagged as prolonged safety stops, and the effectiveness of these procedures has been substantiated *in vivo* (dogs) by Kunkle and Beckman. In-water recompression procedures, similar to the Australian regimens, complement Hawaiian diving practices for all the same reasons.

While the above practices developed by trial-and-error, albeit with seeming principle, venous gas emboli measurements, performed off Catalina by Pilmanis on divers making shallow safety stops, fall into the more *scientific* category perhaps. Contrasting bubble counts following bounce exposures near 100 fsw, with and without zonal stops in the 10-20 fsw range, marked reductions (factors of 4 to 5) in venous gas emboli were noted when stops were made. If, as some suggest, venous gas emboli in bounce diving correlate with bubbles in sites such as tendons and ligaments, then safety stops probably minimize bubble growth in such extravascular locations. In these tests, the sample population was small, so additional validation and testing is warranted.

DECOMPRESSION RISK AND STATISTICS

Systematics And Issues

The systematics of gas exchange, nucleation, bubble growth and elimination, and decompression are so complicated that theories only reflect pieces of the puzzle. Computational algorithms, tables, and manned testing are requisite across a spectrum of activities. And the potential of electronic devices to process tables of information or detailed equations underwater is near maturity, with virtually any algorithm or model amenable to digital implementation. Pressures for even more sophisticated algorithms are expected to grow.

Still computational models enjoy varying degrees of success or failure. More complex models address a greater number of issues, but are harder to codify in decompression tables. Simpler models are easier to codify, but are less comprehensive. Some models are based on first principles, but many are not. Application of models can be subjective in the absence of definitive data, the acquisition of which is tedious, sometimes controversial, and often ambiguous. If deterministic models are abandoned, statistical analysis can address the variability of outcome inherent to random occurrences, but only in manner indifferent to specification of controlling mechanisms. The so called dose-reponse characteristics of statistical analysis are very attractive in the formulation of risk tables. Applied to decompression sickness incidence, tables of comparative risk offer a means of weighing contributing factors and exposure alternatives. At the basis of statistical and probabilistic analyses of decompression sickness is the binomial distribution. The binomial distribution is the fundamental frequency distribution governing random events.

Binomial Distribution

Decompression sickness is a hit, or no hit, situation. Statistics are binary, as in coin tossing. Probabilities of occurrence are determined from the binomial distribution, which measures the numbers of possibilities of occurrence and nonoccurrence in any number of events, given the incidence rate. Specifically, the probability, P , in a random sample of size, N , for n occurrences of decompression sickness and m nonoccurrences, takes the form,

$$P(n) = \frac{N!}{n! m!} p^n q^m , \quad (73)$$

with,

$$n + m = N , \quad (74)$$

p the underlying incidence rate (average number of cases of decompression sickness), and q ,

$$q = 1 - p , \quad (75)$$

the underlying nonincidence. The discrete probability distributions, P , are the individual terms of the binomial expansion of $(p + q)^N$,

$$(p + q)^N = \sum_{n=0}^N P(n) = 1 . \quad (76)$$

In risk analysis, p and q are also the failure and success rates, gleaned, for instance, from random or strategic sampling of arbitrary lot sizes. Obviously, the larger the sample size, the better are the estimates of p or q . Once p or q is determined, the binomial statistics and probabilities are also fixed. The statistical mean, M , and variance, s , are given by,

$$M = \sum_{n=1}^N nP(n) = pN , \quad (77)$$

$$s = \sum_{n=1}^N (n - M)^2 P(n) = pqN , \quad (78)$$

the usual measures of a statistical distribution. The square root of the variance is the standard deviation. The cumulative probability for more than n cases of decompression sickness, $P_{>}(n)$, is written,

$$P_{>}(n) = \sum_{j=n+1}^N P(j) = 1 - \sum_{j=0}^n P(j) , \quad (79)$$

and the probability of less than n cases, $P_{<}(n)$, is similarly,

$$P_{<}(n) = \sum_{j=0}^{n-1} P(j) = 1 - \sum_{j=n}^N P(j) . \quad (80)$$

The probability of nonoccurrence in any set of N trials is simply,

$$P(0) = q^N , \tag{81}$$

while the probability of total occurrence in the same number, N , of trials is given by,

$$P(N) = p^N . \tag{82}$$

Probabilistic Decompression

Table 12 lists corresponding binomial decomposition probabilities, $P(n)$, for 1% and 10% underlying incidence (99% and 90% nonincidence), yielding 0, 1, and 2 or more cases of decompression sickness. The underlying incidence, p , is the (fractional) average of hits.

As the number of trials increases, the probability of 0 or 1 occurrences drops, while the probability of 2 or more occurrences increases. In the case of 5 dives, the probability might be as low as 5%, while in the case of 50 dives, the probability could be 39%, both for $p = 0.01$. Clearly, odds even percentages would require testing beyond 50 cases for an underlying incidence near 1%. Only by increasing the number of trials for fixed incidences can the probabilities be increased. Turning that around, a rejection procedure for 1 or more cases of decompression sickness at the 10% probability level requires many more than 50 dives. If we are willing to lower the confidence of the acceptance, or rejection, procedure, of course, the number of requisite trials drops. Table 12 also shows that the test practice of accepting an exposure schedule following 10 trials without incidence of decompression sickness is suspect, merely because the relative probability of nonincidence is high, near 35%.

Questions as to how safe are decompression schedules have almost never been answered satisfactorily. As seen, large numbers of binary events are required to reliably estimate the underlying incidence. One case of decompression sickness in 30 trials could result from an underlying incidence, p , bounded by 0.02 and 0.16 roughly. Tens more of trials are necessary to shrink those bounds.

Table 12. Probabilities Of Decompression Sickness For Underlying Incidences.

N (dives)	n (hits)	$P(n)$	
		$p = .01$ $q = .99$	$p = .10$ $q = .90$
5	0	.95	.59
	1	.04	.33
	2 or more	.01	.08
10	0	.90	.35
	1	.09	.39
	2 or more	.01	.26
20	0	.82	.12
	1	.16	.27
	2 or more	.02	.61
50	0	.61	.01
	1	.31	.03
	2 or more	.08	.96

Biological processes are highly variable in outcome. Formal correlations with outcome statistics are then generally requisite to validate models against data. Often, this correlation is difficult to firmly establish (couple of percent) with fewer than 1,000 trial observations, while ten percent correlations can be obtained with 30 trials, assuming binomial distributed probabilities. For decompression analysis, this works as a disadvantage, because often the trial space of dives is small. Not discounting the possibly small trial space, a probabilistic approach to the occurrence of decompression sickness is useful and necessary. One very successful approach, developed and tuned by Weathersby, and others for decompression sickness in diving, called maximum likelihood, applies theory or models to diving data and adjusts the parameters until theoretical prediction and experimental data are in as close agreement as possible.

Validation procedures require decisions about uncertainty. When a given decompression procedure is repeated with different subjects, or the same subjects on different occasions, the outcome is not constant. The uncertainty about the occurrence of decompression sickness can be quantified with statistical statements, though, suggesting limits to the

validation procedure. For instance, after analyzing decompression incidence statistics for a set of procedures, a table designer may report that the procedure will offer an incidence rate below 5%, with 90% confidence in the statement. Alternatively, the table designer can compute the probability of rejecting a procedure using any number of dive trials, with the rejection criteria any arbitrary number of incidences. As the number of trials increases, the probability of rejecting a procedure increases for fixed incidence criteria. In this way, relatively simple statistical procedures can provide vital information as to the number of trials necessary to validate a procedure with any level of acceptable risk, or the maximum risk associated with any number of incidences and trials.

One constraint usually facing the statistical table designer is a paucity of data, that is, number of trials of a procedure. Data on hundreds of repetitions of a dive profile are virtually nonexistent, excepting bounce diving perhaps. As seen, some 30-50 trials are requisite to ascertain procedure safety at the 10% level. But 30-50 trials is probably asking too much, is too expensive, or generally prohibitive. In that case, the designer may try to employ global statistical measures linked to models in a more complex trial space, rather than a single profile trial space. Integrals of risk parameters, such as bubble number, supersaturation, separated phase, etc., over exposures in time, can be defined as probability measures for incidence of decompression sickness, and the maximum likelihood method then used to extract appropriate constants.

Maximum Likelihood

We can never measure any physical variable exactly, that is, without error. Progressively more elaborate experimental or theoretical efforts only reduce the possible error in the determination. In extracting parameter estimates from data sets, it is necessary to also try to minimize the error (or data scatter) in the extraction process. A number of techniques are available to the analyst, including the well known maximum likelihood approach.

The measure of any random occurrence, p , can be a complicated function of many parameters, $x = (x_k, k = 1, K)$, with the only constraint,

$$0 \leq p(x) \leq 1 \quad , \quad (83)$$

for appropriate values of the set, x . The measure of nonoccurrence, q , is then by conservation of probability,

$$q(x) = 1 - p(x) \quad , \quad (84)$$

over the same range,

$$0 \leq q(x) \leq 1 \quad . \quad (85)$$

Multivalued functions, $p(x)$, are often constructed, with specific form dictated by theory or observation over many trials or tests. In decompression applications, the parameters, x , may well be the bubble-nucleation rate, number of venous gas emboli, degree of supersaturation, amount of pressure reduction, volume of separated gas, ascent rate, or combinations thereof. Parameters may also be integrated in time in any sequence of events, as a global measure, though such measures are more difficult to analyze over arbitrary trial numbers.

The likelihood of any outcome, Φ , of N trials is the product of individual measures of the form,

$$\Phi(n) = p^n q^m = p^n (1 - p)^m \quad , \quad (86)$$

given n cases of decompression sickness and m cases without decompression sickness, and,

$$n + m = N \quad . \quad (87)$$

The natural logarithm of the likelihood, Ψ , is easier to use in applications, and takes the form,

$$\Psi = \ln \Phi = n \ln p + m \ln (1 - p) \quad , \quad (88)$$

and is maximized when,

$$\frac{\partial \Psi}{\partial p} = 0 \quad . \quad (89)$$

In terms of the above, we then must have,

$$\frac{n}{p} - \frac{m}{1-p} = 0 , \quad (90)$$

trivially requiring,

$$p = \frac{n}{n+m} = \frac{n}{N} , \quad (91)$$

$$1-p = q = \frac{m}{n+m} = \frac{m}{N} . \quad (92)$$

Thus, the likelihood function is maximized when p is the actual incidence rate, and q is the actual nonincidence rate. The multivalued probability functions, $p(x)$, generalize in the maximization process according to,

$$\frac{\partial \Psi}{\partial p} = \sum_{k=1}^K \frac{\partial \Psi}{\partial x_k} \frac{\partial x_k}{\partial p} = 0 , \quad (93)$$

satisfied when,

$$\frac{\partial \Psi}{\partial x_k} = 0 \text{ for } k = 1, K . \quad (94)$$

In application, such constraints are most easily solved on computers, with analytical or numerical methods.

In dealing with a large number of decompression procedures, spanning significant range in depth, time, and environmental factors, an integrated approach to maximum likelihood and risk is necessary. Integral measures, $p(x, t)$ and $q(x, t)$, can be defined over assumed decompression risk, $\zeta(x, t)$,

$$p(x, t) = 1 - \exp \left[- \int_0^t \zeta(x, t') dt' \right] , \quad (95)$$

$$q(x, t) = \exp \left[- \int_0^t \zeta(x, t') dt' \right] , \quad (96)$$

with t' any convenient time scale, and ζ any assumed risk, such as bubble number, saturation, venous emboli count, etc. as mentioned. Employing $p(x, t)$ and $q(x, t)$ in the likelihood function, and then maximizing according to the data, permits maximum likelihood estimation of $\zeta(x, t)$. Such an approach can be employed in decompression table fabrication, yielding good statistical estimates on incidence rates as a function of exposure factors.

Saturation Bends Probability

Many factors contribute to bends susceptibility. Age, obesity, temperature, physical condition, alcohol, and cigarettes are a few. Whatever the contributing factors, the distribution of bends depths for saturation exposures has been characterized in terms of the saturation tension, Q , and ambient pressure, P , by Hills. This characterization is not only of academic interest, but is also useful in assigning formal risk to decompression formats.

The distribution of saturation bends depths, χ , fits a Weibull function. This is true for all breathing mixtures, nitrox, heliox, trimix, etc. If cumulative fraction of air bends cases up to G is χ , the survivor fraction, $1 - \chi$, satisfies,

$$\ln (1 - \chi) = - \left[\frac{G - 14.3}{25.1} \right]^{4.73} \quad (97)$$

for cumulative bends probability, χ , the usual integral over bends risk, ζ , as a function of gradient, G ,

$$\chi = \int_0^G \zeta(G') dG' \quad (98)$$

with saturation bends gradient, G , measured in fsw ,

$$G = Q - P \quad (99)$$

As the gradient grows, the survivor function approaches zero exponentially. The smallest bends gradient is $14.3 fsw$, which can be contrasted with the average value of $26.5 fsw$. The root mean square gradient is $27.5 fsw$. At $27 fsw$, the survivor fraction is 0.96 , while 67% of survivors fall in the range, $26.5 \pm 7.6 fsw$, with $7.6 fsw$ the standard deviation. For gas mixtures other than air, the general form is given by,

$$\ln(1 - \chi) = -\varepsilon \left[\frac{(P - 20.5)}{(P_i - 33.0)} - \frac{1}{f_i} \right]^\delta \quad (100)$$

where f_i is the total volume fraction of inert breathing gases, for $G = P - P_i$, and with ε, δ constants.

The efficiency of the Weibull distribution in providing a good fit to the saturation data is not surprising. The Weibull distribution enjoys success in reliability studies involving multiplicities of fault factors. It obviously extends to any set of hyperbaric or hypobaric exposure data, using any of the many parameter risk variables described above.

Table And Profile Risks

A global statistical approach to table fabrication consists of following a risk measure, or factor p , throughout and after sets of exposures, tallying the incidence of DCI, and then applying maximum likelihood to the risk integral in time, extracting any set of risk constants optimally over all dives in the maximization procedure. In analyzing air and helium data, Weathersby assigned risk as the difference between tissue tension and ambient pressure divided by ambient pressure. One tissue was assumed, with time constant ultimately fixed by the data in ensuing maximum likelihood analysis. The measure of nonincidence, q , was taken to be the exponential of risk integrated over all exposure time,

$$q(\kappa, \tau) = \exp \left[- \int_0^\infty \zeta(\kappa, \tau, t') dt' \right], \quad (101)$$

$$\zeta(\kappa, \tau, t') = \kappa \frac{p(t') - p_a}{p_a}, \quad (102)$$

with κ a constant determined in the likelihood maximization, p_a ambient pressure, and $p(t')$ the instantaneous Haldane tension for tissue with halftime, τ , also determined in the maximization process, corresponding to arbitrary tissue compartments for the exposure data. Other more complex likelihood functions can also be employed, for instance, the separated phase volume according to the varying permeability and reduced gradient bubble models,

$$\zeta(\kappa, \xi, \tau, t') = \kappa \Lambda G(t'), \quad (103)$$

$$\Lambda = \left[1 - \frac{r}{\xi} \right], \quad (104)$$

with Λ the permissible bubble excess, r the bubble radius, G the bubble diffusion gradient (dissolved-free gas), and κ and ξ constants determined in the fit maximization of the data. Another risk possibility is the tissue ratio,

$$\zeta(\kappa, \tau, t') = \kappa \frac{p(t')}{p_a}, \quad (105)$$

a measure of interest in altitude diving applications.

Hundreds of air dives were analyzed using this procedure, permitting construction of decompression schedules with 95% and 99% confidence (5% and 1% bends probability). These tables were published by US Navy investigators, and Table 13 tabulates the corresponding nonstop time limits ($p = 0.05, 0.01$), and also includes the standard US Navy (Workman) limits for comparison. Later re-evaluations of the standard set of nonstop time limits estimate a probability rate of 1.25% for the limits. In actual usage, the incidence rates are below 0.001%, because users do not dive to the limits generally.

Table 13. Nonstop Time Limits For 1% And 5% DCI Probability.

depth d (fsw)	nonstop limit t_n (min) $P = .05$	nonstop limit t_n (min) $P = .01$	nonstop limit t_n (min) US Navy
30	240	170	
40	170	100	200
50	120	70	100
60	80	40	60
70	80	25	50
80	60	15	40
90	50	10	30
100	50	8	25
110	40	5	20
120	40	5	15
130	30	5	10

For the past 10-15 years, a probabilistic approach to assessing risk in diving has been in vogue. Sometimes this can be confusing, or misleading, since definitions or terms, as presented, are often mixed. Also confusing are risk estimates varying by factors of 10 to 1,000, and distributions serving as basis for analysis, also varying in size by the same factors. So, before continuing with a risk analysis of recreational profiles, a few comments are germane.

Any set of statistical data can be analyzed directly, or sampled in smaller chunks. The smaller sets (samples) may or may not reflect the parent distribution, but if the analyst does his work correctly, samples reflecting the parent distribution can be extracted for study. In the case of dive profiles, risk probabilities extracted from sample profiles try to reflect the incidence rate, p , of the parent distribution (N profiles, and p underlying DCI rate). The incidence rate, p , is the most important metric, followed by the shape of the distribution in total as measured by the variance, s . For smaller sample of profile size, $K < N$, we have mean incidences, Q , for sample incidence rate, r ,

$$Q = rK \tag{106}$$

and variance, v ,

$$v = r(1 - r)K \tag{107}$$

By the central limit theorem, the distribution of sample means, Q , is normally distributed about parent (actual) mean, M , with variance, $v = s/K$. Actually, the distribution of sample means, Q , is normally distributed no matter what the distribution of samples. This important fact is the basis for error estimation with establishment of confidence intervals, χ , for r , with estimates denoted, r_{\pm} ,

$$r_{\pm} = r \pm \chi \left[\frac{s}{K} \right]^{1/2} \tag{108}$$

$$0 < \chi < 1 \tag{109}$$

The sample binomial probability, $B(k)$, is analogously,

$$B(k) = \frac{K!}{k! j!} r^k (1 - r)^j \tag{110}$$

with $k + j = K$, for k the number of DCI hits, normalized,

$$\sum_{k=1}^K B(k) = 1 \tag{111}$$

and with property, if $K \rightarrow \infty$, then $B(k) \rightarrow 0$, when, $r \ll 1$.

For example, if 12 cases of DCI are reported in a parent set of 7,896 profiles, then,

$$N = 7896 \quad (112)$$

$$p = \frac{12}{7896} = .0015 \quad (113)$$

Smaller samples might be used to estimate risk, via sample incidence, r , with samples possibly chosen to reduce computer processing time, overestimate p for conservancy sake, focus on a smaller subregion of profiles, or any other reason. Thus, one might nest all 12 DCI incidence profiles in a smaller sample, $K = 1,000$, so that the sample risk, $r = 12/1,000 = 0.012$, is larger than p . Usually though the analyst wishes to mirror the parent distribution in the sample. If the parent is a set of benign, recreational, no decompression, no multiday dive profiles, and the sample mirrors the parent, then both risks, p and r , are reasonably true measures of actual risk associated with recreational diving. If sample distributions chosen are not representative of the class of diving performed, risk estimates are not trustworthy. For instance, if a high risk set of mixed gas decompression profiles were the background against which recreational dive profiles were compared, all estimates would be skewed and faulty (actually underestimated in relative risk, and overestimated in absolute risk). For this parent set, N is large, p is small, with mean, $M = pN = 0.0015 \times 7896 = 12$, and the applicable binomial statistics smoothly transition to Poisson representation, convenient for logarithmic and covariant numerical analysis (on a computer). Additionally, any parent set may be a large sample of a megaset, so that p is itself an estimate of risk in the megaset.

Turns out that our parent distribution above is just that, a subset of larger megaset, namely, the millions and millions of recreational dives performed and logged over the past 30 years, or so. The above set of profiles was collected in training and vacation diving scenarios. The set is recreational (no decompression, no multiday, light, benign) and representative, with all the distribution metrics as listed. For reference and perspective, sets of recreational profiles collected by others (Gilliam, NAUI, PADI, YMCA, DAN) are similar in context, but larger in size, N , and smaller in incidence rate, p . Data and studies reported by many sources quote, $N > 1,000,000$, with, $p < 0.00001 = 0.001\%$. Obviously our set has higher rate, p , though still nominally small, but the same shape. So our estimates will be liberal (overestimate risk).

To perform risk analysis, a risk estimator need be employed. For diving, dissolved gas and phase estimators are useful. Two, detailed earlier, are used here. First is the dissolved gas supersaturation ratio, historically coupled to Haldane models, ϕ ,

$$\phi = \kappa \frac{p - \lambda p_a}{p_a} \quad (114)$$

and second, ψ , is the separated phase, invoked by phase models,

$$\psi = \gamma \left[1 - \frac{r}{\xi} \right] G \quad (115)$$

For simplicity, the asymptotic exposure limit is used in the likelihood integrals for both risk functions,

$$1 - r(\kappa, \lambda) = \exp \left[- \int_0^\infty \phi(\kappa, \lambda, t) dt \right] \quad (116)$$

$$1 - r(\gamma, \xi) = \exp \left[- \int_0^\infty \psi(\gamma, \xi, t) dt \right] \quad (117)$$

with *hit – no hit*, likelihood function, Ω , of form,

$$\Omega = \prod_{k=1}^K \Omega_k \quad (118)$$

$$\Omega_k = r_k^{\delta_k} (1 - r_k)^{1 - \delta_k} \quad (119)$$

where, $\delta_k = 0$ if DCI does not occur in profile, k , or, $\delta_k = 1$ if DCI does occur in profile, k . To estimate κ , λ , γ , and ξ in maximum likelihood, a modified Levermore-Marquardt algorithm is employed (*SNLSE*, Common Los Alamos Applied Mathematical Software Library), just a nonlinear least squares data fit to an arbitrary function (minimization of variance over K datapoints here), with $L1$ error norm. Additionally, using a random number generator for profiles across 1,000 parallel SMP (Origin 2000) processors at LANL, we construct 1,000 subsets, with $K = 2,000$ and $r = 0.006$, for separate likelihood regression analysis, averaging κ , λ , γ , and ξ by weighting the inverse variance.

For recreational diving, both estimators are roughly equivalent, because little dissolved gas has separated into free phases (bubbles). Analysis shows this true for all cases examined, in that estimated risks for both overlap at the 95% confidence level. The only case where dissolved gas and phase estimators differ (slightly here) is within repetitive diving profiles. The dissolved gas estimator cues on gas buildup in the slow tissue compartments (staircasing for repeats within an hour or two), while the phase estimator cues on bubble gas diffusion in the fast compartments (dropping rapidly over hour time spans). This holding true within all recreational diving distributions, we proceed to the risk analysis.

Nonstop limits (NDLs), denoted t_n as before, from the US Navy, PADI, and NAUI Tables, and those employed by the Oceanic decometer provide a set for comparison of relative DCI risk. Listed below in Table 14 are the NDLs and corresponding risks, r_n , for the profile, assuming ascent and descent rates of $60 \text{ fsw}/\text{min}$ (no safety stops). Haldane and RGBM estimates vary little for these cases, and only the phase estimates are included.

Table 14. Risk Estimates For Various NDLs.

$d \text{ (fsw)}$	USN $t_n \text{ (min)}$	PADI $t_n \text{ (min)}$	NAUI $t_n \text{ (min)}$	Oceanic $t_n \text{ (min)}$
35	310 (4.3%)	205 (2.0%)		181 (1.3%)
40	200 (3.1%)	140 (1.5%)	130 (1.4%)	137 (1.5%)
50	100 (2.1%)	80 (1.1%)	80 (1.1%)	80 (1.1%)
60	60 (1.7%)	55 (1.4%)	55 (1.4%)	57 (1.5%)
70	50 (2.0%)	40 (1.2%)	45 (1.3%)	40 (1.2%)
80	40 (2.1%)	30 (1.3%)	35 (1.5%)	30 (1.3%)
90	30 (2.1%)	25 (1.5%)	25 (1.5%)	24 (1.4%)
100	25 (2.1%)	20 (1.3%)	22 (1.4%)	19 (1.2%)
110	20 (2.2%)	13 (1.1%)	15 (1.2%)	16 (1.3%)
120	15 (2.0%)	13 (1.3%)	12 (1.2%)	13 (1.3%)
130	10 (1.7%)	10 (1.7%)	8 (1.3%)	10 (1.7%)

Risks are internally consistent across NDLs at each depth, and agree with the US Navy assessments in Table 2. Greatest underlying and binomial risks occur in the USN shallow exposures. The PADI, NAUI, and Oceanic risks are all less than 2% for this set, thus binomial risks for single DCI incidence are less than 0.02%. PADI and NAUI have reported that field risks (p) across all exposures are less than 0.001%, so considering their enviable track record of diving safety, our estimates are liberal. Oceanic risk estimates track as the PADI and NAUI risks, again, very safely.

Next, the analysis is extended to profiles with varying ascent and descent rates, safety stops, and repetitive sequence. Table 15 lists nominal profiles (recreational) for various depths, exposure and travel times, and safety stops at 5 msw . DCI estimates, r , are tabulated for both dissolved gas supersaturation ratio (ZHL) and bubble number excess (RGBM) risk functions.

Table 15. Dissolved And Separated Phase Risk Estimates For Nominal Profiles.

profile (<i>depth/min</i>)	descent rate (<i>msw/min</i>)	ascent rate (<i>msw/min</i>)	safety stop (<i>depth/min</i>)	<i>r</i> RGBM	<i>r</i> ZHL
14 <i>msw/38 min</i>	18	9	5 <i>msw/3 min</i>	.0034	.0062
19 <i>msw/38 min</i>	18	9	5 <i>msw/3 min</i>	.0095	.0110
37 <i>msw/17 min</i>	18	9	5 <i>msw/3 min</i>	.0165	.0151
18 <i>msw/31 min</i>	18	9	5 <i>msw/3 min</i>	.0063	.0072
	18	9		.0088	.0084
	18	18		.0101	.0135
	18	18	5 <i>msw/3 min</i>	.0069	.0084
17 <i>msw/32 min</i>	18	9	5 <i>msw/3 min</i>		
SI 176 <i>min</i>					
13 <i>msw/37 min</i>	18	9	5 <i>msw/3 min</i>		
SI 174 <i>min</i>					
23 <i>msw/17 min</i>	18	18	5 <i>msw/3 min</i>	.0127	.0232

The ZHL (Buhlmann) NDLs and staging regimens are widespread across decompression meters presently, and are good representation for Haldane risk analysis. The RGBM is newer and more modern (and more physically correct), and is coming online in decometers and associated software. For recreational exposures, the RGBM collapses to a Haldane dissolved gas algorithm. This is reflected in the risk estimates above, where estimates for both models differ little.

Simple comments hold for the analyzed profile risks. The maximum relative risk is 0.0232 for the 3 dive repetitive sequence according to the Haldane dissolved risk estimator. This translates to .2% binomial risk, which is comparable to the maximum NDL risk for the PADI, NAUI, and Oceanic NDLs. Again, this type of dive profile is common, practiced daily on liveboards, and benign. According to Gilliam, the absolute incidence rate for this type of diving is less than 0.02%. Again, our figures overestimate risk.

Effects of slower ascent rates and safety stops are noticeable at the 0.25% to 0.5% level in relative surfacing risk. Safety stops at 5 *m* for 3 *min* lower relative risk an average of 0.3%, while reducing the ascent rate from 18 *msw/min* to 9 *msw/min* reduces relative risk an average of 0.35%.

Staging, NDLs, and other constraints imposed by decometer algorithms are entirely consistent with acceptable and safe recreational diving protocols. The estimated absolute risk associated across all ZHL NDLs and diver staging regimens analyzed herein is less than .232%, and is probably much less in actual practice. That is, we use $p = 0.006$, and much evidence suggests $p < 0.0001$, some ten times safer.

Implicit in such formulations of risk tables are the assumptions that a decompression stress is more likely to produce symptoms if it is sustained in time, and that large numbers of separate events may culminate in the same probability after time integration. Though individual schedule segments may not be replicated enough to offer total statistical validation, categories of predicted safety can always be grouped within subsets of corroborating data. Since the method is general, any model parameter or meaningful index, properly normalized, can be applied to decompression data, and the full power of statistical methods employed to quantify overall risk. While powerful, such statistical methods are neither deterministic nor mechanistic, and cannot predict on first principles. But as a means to table fabrication with quoted risk, such approaches offer attractive pathways for analysis.

Validation of schedules and tables can be effected by a set of procedures based on statistical decompression analysis:

1. select or construct a measure of decompression risk, or a probabilistic model;
2. evaluate as many dives as possible, and especially those dives similar in exposure time, depth, and environmental factors;
3. conduct limited testing if no data is available;
4. apply the model to the data using maximum likelihood;
5. construct appropriate schedules or tables using whatever incidence of decompression sickness is acceptable;

6. release and then collect profile statistics for final validation and tuning.

Questions of what risk is acceptable to the diver vary. Sport and research divers would probably opt for very small risk (0.01% or less), while military and commercial divers might live with higher risk (1%), considering the nearness of medical attention in general. Many factors influence these two populations, but fitness and acclimatization levels would probably differ considerably across them. While such factors are difficult to fold into any table exercise or analysis, the simple fact that human subjects in dive experiments exhibit higher incidences during testing phases certainly helps to lower the actual incidence rate in the field, noted by Bennett and Lanphier.

Reduced Gradient Bubble Model Validation And Testing

Models need validation and testing. Often, strict chamber tests are not possible, economically nor otherwise, and algorithms employ alternate benchmarks and regimens to underscore viability. The following are some supporting the RGBM phase model and (released) nitrox, heliox, and trimix diving tables:

1. counterterror and countermeasures (LANL) exercises have used the RGBM (full up iterative deep stop version) for a number of years, logging some 645 dives on mixed gases (trimix, heliox, nitrox) without incidence of DCI – 35% were deco dives, and 25% were repets (no deco) with at least 2 hr SIs, and in the forward direction (deepest dives first);
2. NAUI Technical Diving has been diving the deep stop version for the past 5 yrs, some estimated 3005 dives, on mixed gases down to 250 *fsw*, without a single DCI hit. Some 15 divers, Fall of 1999, in France used the RGBM to make 2 mixed gas dives a day, without mishap, in cold water and rough seas;
3. modified RGBM recreational algorithms (Haldane imbedded with bubble reduction factors limiting reverse profile, repetitive, and multiday diving), as coded into SUUNTO, ABYSS, Plexus, HydroSpace decometers, lower an already low DCI incidence rate of approximately 1/10,000 or less. More RGBM decompression meters, including mixed gases, are in the works (3 not named at this time);
4. a cadre of divers and instructors in mountainous New Mexico, Utah, and Colorado have been diving the modified (Haldane imbedded again) RGBM at altitude, an estimated 350 dives, without peril. Again, not surprising since the altitude RGBM is slightly more conservative than the usual Cross correction used routinely up to about 8,000 ft elevation, and with estimated DCI incidence less than 1/10,000;
5. within decometer implementations of the RGBM, not a single DCI hit has been reported in nonstop and multi-diving categories, beyond 20,000 dives or more, up to now;
6. some extreme 40 -50 chamber tests for mixed gas RGBM have been works, and less stressful exposures will be addressed shortly – extreme here means 300 *fsw* and beyond;
7. probabilistic decompression analysis of some selected RGBM profiles, calibrated against similar calculations of the same profiles by Duke, help validate the RGBM on a computational basis, suggesting that the RGBM has no more theoretical risk than other bubble or dissolved gas models (Weathersby, Vann, Gerth methodology at USN and Duke).
8. all divers and instructors using RGBM decometers, tables, or NET software have been advised to report individual profiles to DAN Project Dive Exploration (Vann, Gerth, Denoble and many others at Duke);
9. ABYSS is a NET software package that offers the modified RGBM (folded over the Buhlmann ZHL) and soon the full up, deep stop version for any gas mixture, has a fairly large contingent of tech divers already using the RGBM and has not received any reports of DCI, something near 3400 dives;
10. outside of proprietary (commercial) and RGBM Tables, mixed gas tables are a smorgasboard of less applicable Haldane dynamics and discretionary stop insertions, as witnessed by the collective comments of a very vocal and extremely competent, experienced technical diving community.

Because DCI is binomially distributed in incidence probability, many trials are often needed (or other close profiles) to fully validate any model at the 1% level. Additionally, full validation requires DCI incidences, the higher the number, the better, contrary to desired dive outcomes.

OXYGEN DOSE AND TOXICITY

High Pressure Oxygen

Decompression sickness could be avoided by breathing just pure oxygen. And the usage of higher concentrations of oxygen in breathing mixtures not only facilitates metabolic function, but also aids in the washout of inert gases such as nitrogen and helium. Despite the beneficial effects of breathing oxygen at higher concentrations, oxygen proves to be toxic in excessive amounts, and over cumulative time intervals. Too little oxygen is equally detrimental to the diver. As discussed, limits to oxygen partial pressures in breathing mixtures range, 0.16 atm to 1.6 atm, roughly, but symptoms of hypoxia and hyperoxia are dose dependent. Or, in other words, symptom occurrences depend on oxygen partial pressures and exposure times, just like inert gas decompression sickness. The mixed gas diver needs to pay attention not only to helium and nitrogen in staged decompression, but also cumulative oxygen exposure over the dive, and possible underexposure on oxygen depleted breathing mixtures.

The neurotoxic actions of high pressure oxygen are thought to relate directly to biochemical oxidation of enzymes, either those linked to membrane permeability or metabolic pathways. The list below is not exhaustive, but includes the following mechanisms:

1. the inability of blood to remove carbon dioxide from tissue when hemoglobin is oxygen saturated;
2. inhibition of enzymes and coenzymes by lipid peroxides;
3. increased concentration of chemical free radicals which attack cells;
4. oxidation of membranes and structural deterioration reducing electrical permeability for neuron activation;
5. direct oxygen attack on smooth muscle fibres;
6. oxygen induced vasoconstriction in arterioles;
7. elevation of brain temperature due to lack of replacement of oxygen by carbon dioxide in hemoglobin;
8. and, simple chemical kinetic redistribution of cellular carbon dioxide and oxygen with high surrounding oxygen tensions.

Fortunately for the diver, there are ways to avoid complications of hyperoxia. Careful attention to dose (depth-time) limitations for oxygen exposures is needed.

Despite the multiplicity and complexity of the above, limits for safe oxygen exposure are reasonably defined. Table 6 below lists NOAA CNS oxygen exposure time limits, t_x , for corresponding oxygen partial pressures, p_{O_2} . Below 0.5 atm, oxygen toxicity (CNS or pulmonary) is not really a problem.

Table 6. Oxygen Dose-Time Limits

oxygen partial pressure p_{O_2} (atm)	oxygen time limit t_x (min)	oxygen tolerance (OTU) Υ (min)
1.6	45	87
1.5	120	213
1.4	150	244
1.3	180	266
1.2	210	278
1.1	240	279
1.0	300	300
0.9	360	299
0.8	450	295
0.7	570	266
0.6	720	189

The data in Table 6 is easily fitted to a dose time curve, using least squares, yielding,

$$t_x = \exp \left[\frac{3.0 - p_{O_2}}{.36} \right] = 4160 \exp (-2.77 p_{O_2}) \quad (120)$$

or, equivalently,

$$p_{O_2} = 3.0 - .36 \ln (t_x) \quad (121)$$

in the same units, that is p_{O_2} and t_x in *atm* and *min* respectively. The last column tabulates a pulmonary exposure dose, Y , for divers, called the oxygen tolerance unit (OTU), developed by Lambertsen and coworkers at the University of Pennsylvania. Formally, the oxygen tolerance, Y , is given by,

1. maintain single dive OTUs below 1440 *min* on the liberal side, or allow for 690 *min* of that as possible full DCI recompression treatment on the conservative side, that is, 750 *min*;
2. maintain repetitive total dive OTUs below 300 *min*.

The expression is applied to each and all segments of a dive, and summed accordingly for total OTUs, and then benchmarked against the 750 *min* or 300 *min* rough rule. The 750 *min* and 300 *min* OTU rules are not cast in stone in the diving community, and 10% to 25% variations are common, in both conservative and liberal directions. Figure 2 depicts the depth-time relationships for oxygen dose. Formally, for multiple exposures (multilevel, deco, repetitive), the cumulative OTU, Y , is the sum of segment doses, Y_n , with segment times, t_n , and partial oxygen pressures, p_{nO_2} , at each n^{th} segment,

$$Y = \sum_{n=1}^N Y_n = \sum_{n=1}^N \left[\frac{p_{nO_2} - 0.5}{0.5} \right]^{0.83} t_n \quad (122)$$

for N segments. For exceptional and multiple exposures, the USN and University of Pennsylvania suggest the CNS limits summarized in Table 7, where for multiple exposures, N , and segment times, t_{x_n} ,

$$T_x = \sum_{n=1}^N t_{x_n} \quad (123)$$

Table 7. Oxygen Exceptional Exposure Time Limits

oxygen partial pressure p_{O_2} (<i>atm</i>)	single exposure t_x (<i>min</i>)	multiple exposures T_x (<i>min</i>)
2.0	30	
1.9	45	
1.8	60	
1.7	75	
1.6	120	15
1.5	150	180
1.4	180	180
1.3	240	210
1.2	270	240
1.1	300	270
0.9	360	360
0.8	450	450
0.7	570	570
0.6	720	720

Note the severe reduction in multiple oxygen exposure time at 1.6 *atm* in Table 7. For this reason, technical divers generally restrict mixed gas diving exposures to $p_{O_2} \leq 1.6 \text{ atm}$ throughout any sequence of dives.

A similar toxicity unit, Φ , initially introduced by Lambertsen and called the unit pulmonary toxicity dose (UPTD) is closely related to the OTU, Y , and is given by,

$$\Phi = \left[\frac{p_{O_2} - 0.5}{0.5} \right]^{1.2} t \quad (124)$$

and weights oxygen partial pressures more than time in dose estimates. Both are employed in the diving community as useful oxygen depth-time limiters.

For the diver, all the foregoing translates into straightforward oxygen management protocols for both CNS and pulmonary toxicity. They are similar to inert gas management, but individual susceptibilities to oxygen seem to vary more widely, though reported statistics are more scattered. Consider CNS oxygen management first, using the CNS clock as it is popularly termed, and then pulmonary oxygen management, using the OTU as described.

CNS Toxicity Management

The various oxygen time limits, t_x , tabulated in the Tables above, obviously bound exposures, t , at oxygen partial pressure, p_{O_2} . Converting the exposure time to a fraction of the limit, Ξ_n , we can define a CNS oxygen clock, Ξ , that is over N exposure levels,

$$\Xi = \sum_{n=1}^N \Xi_n \quad (125)$$

where,

$$\Xi_n = \frac{t_n}{t_{xn}} \quad (126)$$

for exposure time, t_n , at level, n , with oxygen time limit, t_{xn} . Tabulating Ξ is most easily done by a computer. The prescription might be, depending on degree of conservatism,

$$0.7 \leq \Xi \leq 1.3 \quad (127)$$

and where $\Xi = 1$ is the nominal choice. The fit equation for p_{O_2} and t_x suffices to range estimates of Ξ across all depths.

For repetitive dives, a surface interval penalty, similar to the nitrogen penalty in the USN Tables, can be levied for oxygen. A 90 *min* half-time is employed today, that is, the decay constant for residual oxygen CNS management, λ_{O_2} , is,

$$\lambda_{O_2} = \frac{0.693}{90} = 0.0077 \text{ min}^{-1} \quad (128)$$

For surface interval, t , initial CNS clock, Ξ_i , and for 90 *min* folding time, the penalty (or residual) CNS clock, Ξ , is simply,

$$\Xi = \Xi_i \exp(-0.0077t) \quad (129)$$

The residual value is added to the planned repetitive dive additively, just like nitrogen penalty bottom time.

Pulmonary Toxicity Management

Pulmonary oxygen toxicity, Y , follows a similar management scheme. As described, the total exposure, Y , is the sum of interval exposures, Y_n ,

$$Y = \sum_{n=1}^N Y_n = \sum_{n=1}^N \left[\frac{p_{nO_2} - 0.5}{0.5} \right]^{0.83} t_n \quad (130)$$

and is limited,

$$300 \text{ min} \leq Y \leq 750 \text{ min} \quad (131)$$

depending on desired degree of conservatism, and multiplicity of repetitive dives. Variations of 15% to 25% in the exposure limits are common.

There are many ways to measure oxygen, with devices called oxygen analyzers. They are employed in chemical plants and refineries, hyperbaric chambers, intensive care units, and nurseries. The paramagnetic analyzer is very accurate, and relies on oxygen molecular response to a magnetic field in displacing inert gases from collection chambers. Thermal conductivity analyzers differentiate oxygen and nitrogen conduction properties in tracking temperatures in thermistors, with difference in temperatures proportional to the oxygen concentration. Magnetic wind analyzers combine properties of paramagnetic and thermal analyzers. Polarographic analyzers measure oxygen concentration by resistance changes across permeable oxygen membranes. Galvanic cell analyzers are microfuel cells, consuming oxygen on touch and generating a small current proportional to the amount of oxygen consumed. In all cases, analyzer response is linear in oxygen concentration.

Although it is tempting to avoid problems of oxygen toxicity by maintaining oxygen partial pressures, p_{O_2} , far below toxic limits, this is not beneficial to inert gas elimination (free or dissolved state). Higher levels of inspired oxygen, thus correspondingly lower levels of inert gases, are advantageous in minimizing inert gas buildup and maximizing inert gas washout. Coupled to narcotic potency of helium and nitrogen, and molecular diffusion rates, balancing and optimizing breathing mixtures with decompression requirements is truly a complex and careful technical diving exercise.

ADDITIONAL READING

- Berghage T.E. and Durman D., 1980, *US Navy Air Recompression Schedule Risk Analysis*, *Nav. Med. Res. Bull.* 1, 1-22.
- Bowker A.H. and Lieberman G.J., 1964, *Engineering Statistics*, Engelwood Cliffs: Prentice-Hall.
- Boycott A.E., Damant G.C.C., and Haldane J.S., 1908, *The Prevention Of Compressed Air Illness*, *J. Hyg.* 8, 342-443.
- Buhlmann A.A., 1984, *Decompression/Decompression Sickness*, Berlin: Springer Verlag.
- Gernhardt M.L., Lambertsen C.J., Miller R.G., and Hopkins E., 1990, *Evaluation Of A Theoretical Model Of Tissue Gas Phase Growth And Resolution During Decompression From Air Diving*, *Undersea Biomed. Res.* 17, 95.
- Hamilton R.W., 1975, *Development Of Decompression Procedures For Depths In Excess Of 400 Feet*, *Undersea And Hyperbaric Medical Society Report*, WS: 2-28-76, Bethesda.
- Hempleman H.V., 1952, *A New Theoretical Basis For The Calculation Of Decompression Tables*, *Medical Research Council Report*, UPS 131, London.
- Hennessy T.R. and Hempleman H.V., 1977, *An Examination Of The Critical Released Gas Concept In Decompression Sickness*, *Proc. Royal Soc. London B197*, 299-313.
- Hills B.A., 1977, *Decompression Sickness*, New York: John Wiley And Sons.
- Le Messurier D.H. and Hills B.A., 1965, *Decompression Sickness: A Study Of Diving Techniques In The Torres Strait*, *Hvaldradets Skrifter* 48, 54-84.
- Neal J.G., O'Leary T.R. and Wienke B.R., 1999, *Trimix Diving*, Fort Lauderdale: Underwater Dynamics Incorporated.
- Nishi R.Y., Eatock B.C., Buckingham I.P. and Ridgewell B.A., 1982, *Assessment Of Decompression Profiles By Ultrasonic Monitoring: No Decompression Dives*, *Defense And Civil Institute Of Environmental Medicine Report*, D.C.IEM 82-R-38, Toronto.
- Parzen E., 1970, *Modern Probability Theory And Its Applications*, New York: John Wiley And Sons.
- Powell R.P. and Rogers R.E., 1989, *Doppler Ultrasound Monitoring Of Gas Phase Formation And Resolution In Repetitive Diving*, *Undersea Biomed. Res.* 16, 69.
- Vann R.D., Grimstad J., and Nielsen C.H., 1980, *Evidence For Gas Nuclei In Decompressed Rats*, *Undersea Biomed. Res.* 7, 107-112.
- Weathersby P.K., Survanshi S. and Homer L.D., 1985, *Statistically Based Decompression Tables: Analysis Of Standard Air Dives, 1950-1970*, *Naval Medical Research Institute report*, NMRI 85-16, Bethesda.
- Weathersby P.K., Homer L.D., and Flynn E.T., 1984, *On The Likelihood Of Decompression Sickness*, *J. Appl. Physiol.* 57, 815-825.

- Wienke B.R., 1993, *Diving Above Sea Level*, Flagstaff: Best.
- Wienke B.R., 1994, *Basic Diving Physics And Applications*, Flagstaff: Best.
- Wienke B.R., 1992, *Numerical Phase Algorithm For Decompression Computers And Application*, *Comp. Biol. Med.* 22, 389-406.
- Wienke B.R., 1991, *Basic Decompression Theory And Application*, Flagstaff: Best.
- Wienke B.R., 1990, *Reduced Gradient Bubble Model*, *Int. J. Biomed. Comp.* 26, 237-256.
- Wienke B.R., 1986, *DECOMP: Computational Package For Nitrogen Transport Modeling In Tissues*, *Comp. Phys. Comm.* 40, 327-336.
- Workman R.D., 1965, *Calculation Of Decompression Schedules For Nitrogen-Oxygen And Helium-Oxygen Dives*, *USN Experimental Diving Unit Report, NEDU 6-65*, Washington DC
- Yount D.E. and Hoffman DC, 1986, *On The Use Of A Bubble Formation Model To Calculate Diving Tables*, *Aviat. Space Environ. Med.* 57, 149-156.
- Yount D.E., 1979, *Skins Of Varying Permeability: A Stabilization Mechanism For Gas Cavitation Nuclei*, *J. Acoust. Soc. Am.* 65, 1431-1439.
- Yount D.E. and Strauss R.H., 1976, *Bubble Formation In Gelatin: A Model For Decompression Sickness*, *J. Appl. Phys.* 47, 5081-5089.